Stable loosely-coupled-type algorithm for fluid–structure interaction in blood flow

Giovanna Guidoboni [a,*], Roland Glowinski [a,b], Nicola Cavallini [a,c], Suncica Canic [a]

[a] Department of Mathematics, University of Houston, PGH 651, Houston, TX 77204-3476, USA
[b] Laboratoire Jacques-Louis Lions, Université P. et M. Curie, 4 Place Jussieu, 75005 Paris, France
[c] Center of Mathematics for Technology, University of Ferrara, Building B, Scientific-Technological Campus, via Saragat 1, 44100 Ferrara, Italy

ABSTRACT

We introduce a novel loosely coupled-type algorithm for fluid–structure interaction between blood flow and thin vascular walls. This algorithm successfully deals with the difficulties associated with the "added mass effect", which is known to be the cause of numerical instabilities in fluid–structure interaction problems involving fluid and structure of comparable densities. Our algorithm is based on a time-discretization via operator splitting which is applied, in a novel way, to separate the fluid sub-problem from the structure elastodynamics sub-problem. In contrast with traditional loosely-coupled schemes, no iterations are necessary between the fluid and structure sub-problems; this is due to the fact that our novel splitting strategy uses the "added mass effect" to stabilize rather than to destabilize the numerical algorithm. This stabilizing effect is obtained by employing the kinematic lateral boundary condition to establish a tight link between the velocities of the fluid and of the structure in each sub-problem. The stability of the scheme is discussed on a simplified benchmark problem and we use energy arguments to show that the proposed scheme is unconditionally stable. Due to the crucial role played by the kinematic lateral boundary condition, the proposed algorithm is named the "kinematically coupled scheme".

Published by Elsevier Inc.

1. Introduction

The study of the flow of a viscous, incompressible fluid through a compliant (elastic or viscoelastic) channel is of interest to many applications. A major application is blood flow in human arteries. Understanding fluid–structure interaction between blood flow and vascular tissue, the wave propagation that it causes in the arterial walls, local hemodynamics and wall shear stress is important in understanding the mechanisms leading to various complications in cardiovascular function.

Fluid–structure interaction between blood flow and vascular tissue is particularly complicated due to the following distinctive features of the problem: (1) The coupling between blood and vascular tissue is highly nonlinear due to the fact that the ratio between the densities of blood and tissue is roughly equal to one. In contrast with other fluid–structure interactions such as those arising in aeroelasticity, in this problem the structure (tissue) is relatively "light" and therefore "sensitive" to the small variations in the fluid forcing giving rise to numerical instabilities. (2) The coupled problem embodies a competition between the hyperbolic effects, associated with wave propagation in the structure, and the parabolic effects, associated

* Corresponding author.
E-mail addresses: gio@math.uh.edu (G. Guidoboni), roland@math.uh.edu (R. Glowinski), nicolauh@math.uh.edu (N. Cavallini), canic@math.uh.edu (S. Canic).

with the viscous dissipation in the fluid (and in the structure, if the structure is viscoelastic). A sophisticated combination of the hyperbolic and parabolic techniques is required for the analytical and numerical study of the problem.

Several techniques have been proposed in the literature for the numerical solution of fluid–structure interaction problems. The best known are the Immersed Boundary Method [19,24,40,43,47,48] and the Arbitrary Lagrangian Eulerian (ALE) method [17,34,36,39,49–51]. We further mention the Fictitious Domain Method in combination with the mortar element method or ALE approach [1,52] and the methods recently proposed for the use in blood flow application such as the Lattice Boltzmann method [18,20,37,38], the Level Set method [14] and the Coupled Momentum method [23].

To date, only *strongly coupled* (monolithic, implicit) algorithms seem applicable to blood flow simulations [4,5,16,23,26,44,54]. Unfortunately, they are generally quite expensive in terms of computational time, programming time and memory requirements, since they require solving a sequence of nonlinear, strongly coupled problems using, e.g. fixed point and Newton's methods [4,5,13,16,22,34,42,44], or Steklov–Poincaré-based domain decomposition methods [15].

The multi-physics features of the blood flow problem strongly suggest to employ partitioned (or staggered) numerical algorithms, in which the coupled fluid–structure interaction problem is split into a pure fluid sub-problem and a pure structure sub-problem. When the density of the structure is much larger than the density of the fluid, as is the case in aeroelasticity, it is sufficient to solve, at every time step, the fluid sub-problem and the structure sub-problem only once. Algorithms which utilize only one fluid and one structure solution at every time step are also known as *loosely coupled* (explicit) algorithms. Unfortunately, when fluid and structure have comparable densities, as is the case with blood and vascular tissue, this approach suffers from severe stability issues due to the improper resolution of the energy balance at the interface, also known as "added mass effect", as shown in [11]. On the other hand, iterating several times between fluid and structure at every time step is computationally expensive and, additionally, suffers from convergence issues for certain parameter values [11,44].

To get around these difficulties, several new methods have recently been proposed.

The method proposed in [2] is based on the classical approach of splitting the coupled problem into the pure fluid and pure structure sub-problems, with the goal of improving the convergence rate of the iterations between the sub-problems by introducing novel transmission conditions. More precisely, instead of using the traditional Dirichlet–Neumann transmission conditions (in which the fluid is solved with a Dirichlet boundary condition at the interface given by the structure velocity, and the structure is solved with a Neumann boundary condition at the interface given by the fluid stress), the authors propose a set of Robin-type transmission conditions. These conditions are obtained in an *ad hoc* manner as a linear combination of the kinematic and dynamic interface conditions. They introduce an artificial redistribution of the fluid stress on the interface between the fluid and the structure sub-problems which gets around the difficulty associated with the added mass effect. A similar approach was previously proposed in [45], where it was shown that, in the case of a simple algebraic membrane model for the structure, the structure can be "embedded" into the fluid problem leading to a Robin boundary condition.

A different stabilizing strategy for explicit schemes for fluid–structure interaction problems was proposed in [8]. Here a coupled discrete formulation based on Nitsche's method [33] was presented, with a time penalty term giving L^2-control on the fluid pressure variations at the interface.

In [21] a different strategy to decouple fluid–structure interaction problems was proposed to get around the difficulties related to the "added mass effect": the computation of the fluid velocity is decoupled from the strongly coupled fluid–structure system which only involves the pressure and structure unknowns. In [21], this method was combined with a Chorin–Temam projection scheme, while in [3,49] the same method was combined with an algebraic splitting which allows the use of other solution strategies, such as the Yosida method.

In the present article we introduce a loosely coupled-type scheme that is fundamentally different from all the schemes presented so far and which possesses the following *appealing features* over the existing schemes:

1. The fluid and structure problems are split (in a novel way) and exisiting solvers can be easily used.
2. No iterations between the fluid and structure sub-problems are required.
3. The transmission conditions between fluid and structure sub-problems are a natural consequence of the coupled problem and do not need to be artificially tuned.
4. The fluid stress at the interface does not need to be computed explicitly.

These features have been achieved by performing a time-discretization via *operator splitting* that

1. Uses the kinematic lateral boundary condition to establish a tight link between the fluid velocity and the structure velocity.
2. Isolates the purely elastic portion of the structure equations without the hydrodynamic load.
3. Treats the hydrodynamic load on the structure together with the fluid.

The crucial role of the kinematic condition for the stability of the proposed algorithm motivates its name: *kinematically coupled scheme*.

More precisely, we consider a fluid–structure interaction problem that couples the Navier–Stokes equations for an incompressible, viscous fluid with the equations modeling an elastic or a viscoelastic thin shell or membrane which serves as a

(lateral) boundary of the fluid domain. The proposed scheme is based on a novel *operator splitting* approach using the Lie's operator splitting method. The main novelty lies in the way how the operator splitting is performed. Instead of treating the equation for the structure dynamics as a whole, we split it into two parts: the hydrodynamic load exerted by the fluid on the structure (together with the viscoelastic terms if the structure is viscoelastic) and the purely elastic part without the hydro-dynamic load. Then, we build our algorithm on two main sub-problems: a *fluid sub-problem* in which the hydrodynamic load on the structure (and the structure viscoelasticity) is taken as data for the fluid velocity on the boundary via a novel bound-ary condition that involves fluid acceleration, and an *elastodynamics sub-problem* driven only by the initial condition, namely by the trace of the fluid velocity at the boundary just computed in the fluid sub-problem.

By this splitting, and in particular by the inclusion of the hydrodynamic load to the structure into the fluid sub-problem, the energy balance is maintained at the time-discrete level, thereby avoiding the "added-mass effect". This is a crucial point of this method which, as discussed in Section 6, is *unconditionally stable*.

It has been our experience that it is important for the stability and accuracy of splitting schemes to treat properly the non-dissipative sub-steps. Indeed, the elastic part of the structure equation is essentially hyperbolic, and therefore non-dissipa-tive, and we take advantage of the operator splitting technique to treat it in a separate sub-step where we can use a non-dissipative solver. This approach was also used in [32] where a fluid–structure interaction problem on a fixed fluid domain was considered. In the same spirit of distinguishing the *hyperbolic* from the *parabolic* part of the problem, we further split the fluid sub-problem into one parabolic step (the Stokes problem) and two hyperbolic steps (fluid advection and ALE advection).

Numerical experiments confirm that our method is stable even in the case when fluid and structure have comparable densities. Our results are in very good agreement with those obtained using strongly coupled schemes.

Our paper is organized as follows: the mathematical problem is formulated in Section 2. In Section 3 we introduce the time-discretization of the underlying fluid–structure interaction problem. In Section 4 we discuss our strategies for solving the underlying sub-problems and in Section 5 we show several numerical results pertinent to the problem. In Section 6 we discuss the stability properties of the scheme and we conclude the paper by Section 7 where remarks about the scheme's features and its drawbacks are discussed.

2. The mathematical model

We consider the flow of an incompressible, viscous fluid in a two-dimensional, axially symmetric channel of length L, with thin, deformable walls. See Fig. 1. We denote the horizontal and vertical coordinates by x_1 and x_2, respectively. In this article we assume that the horizontal displacement of the lateral boundary, which is at reference height $x_2 = H$, is negligible, and we denote the vertical displacement by η. Without loss of generality, we consider only the upper half of the fluid domain supplemented by a symmetry boundary condition at the axis of symmetry. Thus, we define the fluid domain $\Omega(t)$ to be

$$\Omega(t) = \{(x_1, x_2) \in \mathbb{R}^2 | x_1 \in (0, L), x_2 \in (0, H + \eta(x_1, t))\}, \tag{1}$$

with the lateral (top) boundary denoted by

$$\Gamma(t) = \{(x_1, x_2) \in \mathbb{R}^2 | x_1 \in (0, L), x_2 = H + \eta(x_1, t)\}. \tag{2}$$

The fluid flow is governed by the Navier–Stokes equations:

$$\varrho_f \left(\frac{\partial \mathbf{u}}{\partial t} + \mathbf{u} \cdot \nabla \mathbf{u} \right) = \nabla \cdot \boldsymbol{\sigma}, \quad \nabla \cdot \mathbf{u} = 0 \quad \text{in } \Omega(t) \text{ for } t \in (0, T), \tag{3}$$

where $\mathbf{u} = (u_1, u_2)$ is the fluid velocity, p is the fluid pressure, ϱ_f is the fluid density, and $\boldsymbol{\sigma}$ is the fluid stress tensor. We as-sume that the fluid is Newtonian so that the fluid stress tensor is given by $\boldsymbol{\sigma} = -p\mathbf{I} + 2\mu\mathbf{D}(\mathbf{u})$, where μ is the fluid viscosity and $\mathbf{D}(\mathbf{u})$ is the rate-of-strain tensor $\mathbf{D}(\mathbf{u}) = (\nabla \mathbf{u} + (\nabla \mathbf{u})^T)/2$.

We suppose that the flow is driven by a time-dependent pressure drop, imposed by prescribing the normal component of the stress at the inlet and outlet sections:

$$\boldsymbol{\sigma}\mathbf{n}(0, x_2, t) = -\bar{p}(t)\mathbf{n}, \quad \boldsymbol{\sigma}\mathbf{n}(L, x_2, t) = \mathbf{0} \quad \text{on } (0, H) \times (0, T). \tag{4}$$
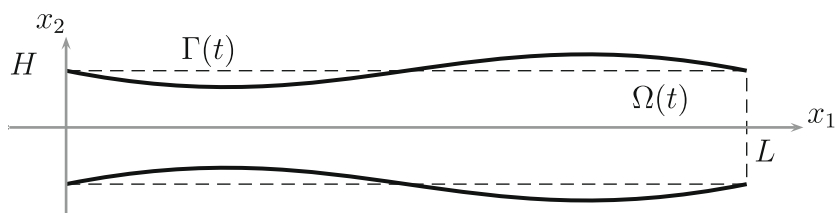

Fig. 1. A sketch of the flow region.

Condition (4) is easier to implement than imposing just the pressure. This kind of boundary condition has been widely used in blood flow modeling [2,35,44,45,49,53].

At the bottom boundary $x_2 = 0$ the following symmetry boundary conditions are imposed:

$$\frac{\partial u_1}{\partial x_2}(x_1, 0, t) = 0, \quad u_2(x_1, 0, t) = 0 \quad \text{on } (0, L) \times (0, T). \tag{5}$$

The upper portion of the domain boundary $\Gamma(t)$ represents the deformable channel wall. In the present article, we assume that $\Gamma(t)$ behaves like a linearly viscoelastic thin shell, undergoing only transversal displacement. The dynamics of $\Gamma(t)$ is modeled by

$$\varrho_s h_s \frac{\partial^2 \eta}{\partial t^2} + C_0 \eta - C_1 \frac{\partial^2 \eta}{\partial x_1^2} + D_0 \frac{\partial \eta}{\partial t} - D_1 \frac{\partial^3 \eta}{\partial t \partial x_1^2} = f_2 \quad \text{on } (0, L) \times (0, T), \tag{6}$$

where ϱ_s is the wall (structure) density, h_s is the wall thickness, C_0 and C_1 are the elastic constants, D_0 and D_1 are the viscoelastic constants, and f_2 is the x_2-projection of the force applied to the structure [9,10,50]. In this problem, the structure dynamics is governed by the time-dependent fluid stress. Thus, f_2 is given by the x_2-projection of the normal fluid stress to the boundary $\Gamma(t)$:

$$f_2 = -\sqrt{1 + \left(\frac{\partial \eta}{\partial x_1}\right)^2} \, \boldsymbol{\sigma} \mathbf{n} \cdot \mathbf{e}_2 \quad \text{on } \Gamma(t) \text{ for } t \in (0, T), \tag{7}$$

where $\mathbf{e}_2 = (0, 1)$. The term with the square-root corresponds to the Jacobian of the transformation between the Eulerian framework used in the description of the fluid flow equations (3) and the Lagrangian framework used in the description of the structure equations (6). Eq. (6) with f_2 given by (7) describes balance of forces (structure and fluid forces at $\Gamma(t)$) and it represents the *dynamic coupling condition* between the fluid and the structure.

The second coupling condition between the fluid and the structure is given by the *kinematic coupling condition* which describes the continuity of the kinematic quantities such as the horizontal and vertical components of the velocity. The continuity of the velocity on $\Gamma(t)$ gives:

$$u_1 = 0, \quad u_2 = \frac{\partial \eta}{\partial t} \quad \text{on } \Gamma(t) \quad \text{for } t \in (0, T). \tag{8}$$

This embodies the no-slip boundary condition at the lateral boundary $\Gamma(t)$.

To complete the problem, we prescribe the boundary conditions for η:

$$\eta(0, t) = \eta(L, t) = 0 \quad \text{on } (0, T), \tag{9}$$

and the initial conditions for the fluid velocity $\mathbf{u}$, the structure displacement η and the structure velocity $\partial \eta / \partial t$:

$$\mathbf{u} = \mathbf{0}, \quad \eta = 0, \quad \frac{\partial \eta}{\partial t} = 0 \quad \text{at } t = 0. \tag{10}$$

The mathematical model (3)–(10) has become a standard benchmark problem for testing numerical strategies to solve the fluid–structure interaction arising in blood flow applications. In this paper, we are using this benchmark problem to explain and validate our method, even though more realistic geometries and elasticity models can be handled by our splitting algorithm without major changes (see Section 3.2, Remark 7).

3. Time-discretization via operator splitting

In this section we discuss the time-discretization of problem (3)–(10) using a strategy based on operator splitting. Operator splitting methods have been widely used for the time-discretization of initial value problems (see e.g. [27,28,41] and the references therein). They are based on the idea of first isolating the main difficulties of the problem and then solving them separately in different (fractional) time steps. The resulting algorithm has a simple modular structure, where the communication between modules is limited to the initial conditions. As a consequence, it is possible to use exisiting solvers (if available) as *black boxes* to solve each sub-step, and, in particular, it is possible to use different time steps and different space discretizations for the different sub-problems.

The application of the operator splitting technique to the time-discretization of problem (3)–(10) is challenging and nonstandard for two reasons. One is related to the fact that Eq. (6) for the wall dynamics contains second-order derivatives in time, while the theory of operator splitting is properly developed only for first-order initial value problems [7]. The second reason is related to the fact that the fluid domain changes in time as a result of the interaction between the fluid flow and the wall (structure) giving rise to the complications in splitting the problem on a moving domain.

To get around the difficulty associated with the fact that the structure equations incorporate the second-order time derivative, we use the kinematic lateral boundary condition (8) to relate the wall acceleration $\partial^2 \eta / \partial t^2$ to the fluid acceleration at the moving boundary $\partial(u_2|_{\Gamma(t)})/\partial t$, see Eq. (20). This has profound consequences on the stability of the algorithm, as discussed in Section 6.

To get around the difficulty associated with the fact that the fluid domain changes in time, we use an ALE-method [44]. More precisely, a family of mappings is introduced which, for each time $t \in (0, T)$, maps the current domain $\Omega(t)$ into a fixed reference domain $\widehat{\Omega}$. As a consequence, the nonlinearities associated with the domain motion clearly appear as nonlinear terms within the equations and the boundary conditions of the remapped problem, while the domain $\widehat{\Omega}$ remains fixed. Applying the operator splitting to this remapped problem (instead of the problem written in the time-dependent domain $\Omega(t)$) guarantees a proper treatment of the nonlinearities deriving from the domain motion. Once the splitting is done, we can solve the corresponding sub-problems on the fixed or on the deformed physical domain depending on which of the two approaches is more convenient.

We mention here that this splitting approach is different from the one studied in [3] where an *algebraic splitting* is performed after the space and time-discretization and linearization of the underlying fluid–structure interaction problem are performed. In our approach, the splitting is performed at the differential level thereby allowing the use of the already existing solvers for the calculation of the solutions of the differential sub-problems.

We begin by first describing the ALE method and deriving a first-order formulation of problem (3)–(10) in the fixed reference domain. Then, in Section 3.2 we introduce the time discretization via operator splitting leading to the kinematically coupled scheme.

3.1. ALE-mapping and first-order formulation

Let $\mathcal{A}_t$ be a family of mappings which at each time $t \in (0, T)$ maps the current domain $\Omega(t)$ into the reference domain $\widehat{\Omega} = (0, L) \times (0, H)$ defined by

$$
\begin{aligned}
&\mathcal{A}_t : \Omega(t) \subset \mathbb{R}^2 \ \rightarrow \ \widehat{\Omega} \subset \mathbb{R}^2 \\
&\mathbf{x} = (x_1, x_2) \ \rightarrow \ \boldsymbol{\xi} = (\xi_1, \xi_2) = \mathcal{A}_t(\mathbf{x}) = \begin{cases} \xi_1 = x_1 \\ \xi_2 = \frac{H}{H+\eta(x_1,t)} x_2, \end{cases}
\end{aligned}
\tag{11}
$$

see Fig. 2. We observe that the deformable, lateral boundary $\Gamma(t)$ is mapped into

$$
\widehat{\Gamma} = \{ \boldsymbol{\xi} \in \mathbb{R}^2 | \xi_1 \in (0, L), \xi_2 = H \}.
\tag{12}
$$

It is clear that this transformation is well defined as long as $H + \eta(x_1, t) > 0$, which is the case for the flow regime we are interested in.

Let $f = f(\mathbf{x}, t)$ be a function defined on $\Omega(t) \times (0, T)$ and $\hat{f} = \hat{f}(\boldsymbol{\xi}, t) = f(\mathcal{A}_t^{-1}(\boldsymbol{\xi}), t)$ the corresponding function defined on $\widehat{\Omega} \times (0, T)$. It follows from the chain rule that

$$
\frac{\partial f}{\partial t} = \frac{\partial \hat{f}}{\partial t} + \mathbf{w} \cdot \widehat{\nabla} \hat{f},
\tag{13}
$$

where the domain velocity $\mathbf{w}$ is given by

$$
\mathbf{w}(\boldsymbol{\xi}, t) = \frac{\partial \mathcal{A}_t(\mathbf{x})}{\partial t} \bigg|_{\mathbf{x}=\mathcal{A}_t^{-1}(\boldsymbol{\xi})} = \frac{\partial \boldsymbol{\xi}}{\partial t},
\tag{14}
$$

and $\widehat{\nabla} = \nabla_{\boldsymbol{\xi}}$. By using the kinematic lateral boundary condition (8) the domain velocity can be expressed as

$$
\mathbf{w}(\boldsymbol{\xi}, t) = -\frac{\xi_2}{H+\eta(\xi_1,t)} \hat{u}_2(\xi_1, H, t) \mathbf{e}_2.
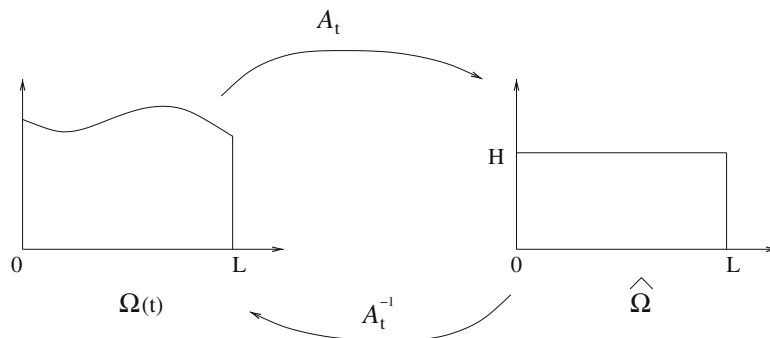\tag{15}
$$

The fluid equations then become:

Fig. 2. $\mathcal{A}_t$ maps the current domain $\Omega(t)$ into the reference domain $\widehat{\Omega}$.

$$\varrho_f\left(\frac{\partial \hat{\mathbf{u}}}{\partial t} + \mathbf{w} \cdot \hat{\nabla}\hat{\mathbf{u}} + \hat{\mathbf{u}} \cdot \hat{\nabla}\hat{\mathbf{u}}\right) = \hat{\nabla} \cdot \hat{\boldsymbol{\sigma}}, \quad \hat{\nabla} \cdot \hat{\mathbf{u}} = 0, \quad \text{in } \widehat{\Omega} \times (0, T), \tag{16}$$

while the kinematic and dynamic lateral boundary conditions on $\widehat{\Gamma}$ read as follows:

$$\hat{u}_1|_{\widehat{\Gamma}} = 0 \quad \text{on } (0, L) \times (0, T), \tag{17}$$

$$\frac{\partial \eta}{\partial t}(\xi_1, t) = \hat{u}_2|_{\widehat{\Gamma}} \quad \text{on } (0, L) \times (0, T), \tag{18}$$

$$\varrho_s h_s \frac{\partial^2 \eta}{\partial t^2} + C_0 \eta - C_1 \frac{\partial^2 \eta}{\partial x_1^2} + D_0 \frac{\partial \eta}{\partial t} - D_1 \frac{\partial^3 \eta}{\partial t \partial x_1^2} = \hat{f}_2|_{\widehat{\Gamma}} \quad \text{on } (0, L) \times (0, T), \tag{19}$$

where $\hat{u}_1|_{\widehat{\Gamma}} = \hat{u}_1(\xi_1, H, t), \hat{u}_2|_{\widehat{\Gamma}} = \hat{u}_2(\xi_1, H, t)$ and $\hat{f}_2 = -\sqrt{1 + (\partial_{\xi_1}\eta)^2}\,\widehat{\boldsymbol{\sigma}\mathbf{n}}|_{\widehat{\Gamma}}\mathbf{e}_2$. To write the problem as a first-order system we use (18) in (19) to obtain the dynamic lateral boundary condition of the form:

$$\varrho_s h_s \frac{\partial(\hat{u}_2|_{\widehat{\Gamma}})}{\partial t} + C_0 \eta - C_1 \frac{\partial^2 \eta}{\partial x_1^2} + D_0 \hat{u}_2|_{\widehat{\Gamma}} - D_1 \frac{\partial^2(\hat{u}_2|_{\widehat{\Gamma}})}{\partial x_1^2} = \hat{f}_2|_{\widehat{\Gamma}} \quad \text{on} \quad (0, L) \times (0, T). \tag{20}$$

Now that the problem is in a first-order form and it is defined on a fixed reference domain, we can use it as a starting point for the time-discretization via operator splitting. Before we present the details of the time-discretization, we summarize the entire problem on the reference domain $\widehat{\Omega}$ in first-order form.

Summary of the problem in the fixed reference domain in first-order form:

$$\begin{cases} \varrho_f\left(\frac{\partial \hat{\mathbf{u}}}{\partial t} + \mathbf{w} \cdot \hat{\nabla}\hat{\mathbf{u}} + \hat{\mathbf{u}} \cdot \hat{\nabla}\hat{\mathbf{u}}\right) = \hat{\nabla} \cdot \hat{\boldsymbol{\sigma}}, \quad \hat{\nabla} \cdot \hat{\mathbf{u}} = 0 \quad \text{in } \widehat{\Omega} \times (0, T) \\[2mm] \frac{\partial \eta}{\partial t}(\xi_1, t) = \hat{u}_2|_{\widehat{\Gamma}} \quad \text{on } (0, L) \times (0, T), \\[2mm] \varrho_s h_s \frac{\partial(\hat{u}_2|_{\widehat{\Gamma}})}{\partial t} + C_0 \eta - C_1 \frac{\partial^2 \eta}{\partial x_1^2} + D_0 \hat{u}_2|_{\widehat{\Gamma}} - D_1 \frac{\partial^2(\hat{u}_2|_{\widehat{\Gamma}})}{\partial x_1^2} = \hat{f}_2|_{\widehat{\Gamma}} \quad \text{on } (0, L) \times (0, T), \end{cases} \tag{21}$$

Boundary conditions:

$$\hat{u}_1|_{\widehat{\Gamma}} = 0 \quad \text{on } (0, L) \times (0, T), \tag{22}$$

$$\left.\frac{\partial \hat{u}_1}{\partial \xi_2}\right|_{\xi_2=0} = \hat{u}_2|_{\xi_2=0} = 0 \quad \text{on } (0, L) \times (0, T), \tag{23}$$

$$\hat{u}_2(0, H, t) = \hat{u}_2(L, H, t) = 0, \quad \eta(0, t) = \eta(L, t) = 0 \quad \text{on } (0, T), \tag{24}$$

$$\widehat{\boldsymbol{\sigma}\mathbf{n}}|_{\xi_1=0} = -\bar{p}(t)\hat{\mathbf{n}}, \quad \widehat{\boldsymbol{\sigma}\mathbf{n}}|_{\xi_1=L} = \mathbf{0} \quad \text{on } (0, H) \times (0, T). \tag{25}$$

Initial conditions:

$$\hat{\mathbf{u}}|_{t=0} = \mathbf{0}, \quad \eta|_{t=0} = 0, \quad \left.\frac{\partial \eta}{\partial t}\right|_{t=0} = 0 \quad \text{on } \widehat{\Omega}. \tag{26}$$

3.2. Operator-splitting scheme

We approximate problem (21)–(26) in time by using the Lie's scheme [27,28]. The Lie's scheme can be summarized as follows. Consider the following initial value problem:

$$\begin{aligned} &\frac{\partial \phi}{\partial t} + A(\phi) = 0 \text{ in } (0, T), \\ &\phi(0) = \phi_0, \end{aligned} \tag{27}$$

where A is a (nonlinear) operator from a Hilbert space into itself. Suppose that operator A has a non-trivial decomposition

$$A = \sum_{i=1}^{I} A_i. \tag{28}$$

Then, the solution of the initial value problem (27) can be approximated via the following scheme:

Let $\Delta t > 0$ be a time-discretization step. Denote $t^n = n\Delta t$ and let ϕ^n be an approximation of $\phi(t^n)$. Set $\phi^0 = \phi_0$. Then, for $n \geqslant 0$ compute ϕ^{n+1} by solving

$$\begin{aligned} &\frac{\partial \phi_i}{\partial t} + A_i(\phi_i) = 0 \text{ in } (t^n, t^{n+1}), \\ &\phi_i(t^n) = \phi^{n+(i-1)/I}, \end{aligned} \tag{29}$$

and then set $\phi^{n+i/I} = \phi_i(t^{n+1})$, for $i = 1, \ldots, I$.

This method is first-order accurate. More precisely, if $((27))$ is defined on a finite-dimensional space and if the operators A_i are smooth enough, then $\|\phi(t^n) - \phi^n\| = O(\Delta t)$. Problem (21)–(26) can be thought as the analogous to problem (27), where ϕ is the array of the unknowns $\hat{\mathbf{u}}$, η and $\hat{u}_2|_{\widehat{\Gamma}}$, while A is a multivalued nonlinear differential operator. There is not a unique way to decompose the operator A, see formula (28), and different choices may lead to the solution of different sub-problems, see problems (29).

Our strategy is to solve separately the following problems:

1. Time-dependent Stokes problem with a suitable boundary condition involving the structure velocity (i.e. the terms involving $\hat{u}_2|_{\widehat{\Gamma}}$ and its derivatives), and the fluid stress at the boundary (i.e. the term $\hat{f}_2|_{\widehat{\Gamma}}$).
2. Fluid advection.
3. ALE-advection.
4. Elastodynamics of the structure (ignoring the viscoelastic terms and fluid stress on the structure).

Notice that the dynamics of the structure is split into its viscoelastic part and the purely elastic part. The viscoelastic part *and* the fluid stress to the structure are taken into account in the first step together with the Stokes problem for the fluid flow. This is in contrast with the classical partitioned schemes that split the underlying multi-physics problem based on the different physical models thereby completely separating the fluid dynamics from the structure dynamics, see e.g. [11]. In our method, the fluid and the structure are coupled at all times through the kinematic lateral boundary condition, while the problem is split into its dissipative part, presented in Step 1, and the remaining non-dissipative part, described in Steps 2–4.

Details of the splitting are presented next.

Step 1. The Stokes problem with the viscoelasticity of the structure and the fluid stress exerted on the structure:

Find $\hat{\mathbf{u}}, \hat{p}$, and η such that

$$
\begin{cases}
\varrho_f \dfrac{\partial \hat{\mathbf{u}}}{\partial t} = \hat{\nabla} \cdot \hat{\boldsymbol{\sigma}}, \quad \hat{\nabla} \cdot \hat{\mathbf{u}} = 0 \quad \text{in } \widehat{\Omega} \times (t^n, t^{n+1}) \\
\dfrac{\partial \eta}{\partial t}(\xi_1, t) = 0 \quad \text{on } (0, L) \times (t^n, t^{n+1}), \\
\varrho_s h_s \dfrac{\partial (\hat{u}_2|_{\widehat{\Gamma}})}{\partial t} + D_0 \hat{u}_2|_{\widehat{\Gamma}} - D_1 \dfrac{\partial^2 (\hat{u}_2|_{\widehat{\Gamma}})}{\partial x_1^2} = \hat{f}_2|_{\widehat{\Gamma}} \quad \text{on } (0, L) \times (t^n, t^{n+1}),
\end{cases}
\tag{30}
$$

with the boundary conditions:

$$
\hat{u}_1|_{\widehat{\Gamma}} = 0 \quad \text{on } (0, L) \times (t^n, t^{n+1}),
\tag{31}
$$

$$
\left.\dfrac{\partial \hat{u}_1}{\partial \xi_2}\right|_{\xi_2=0} = 0, \quad \hat{u}_2|_{\xi_2=0} = 0 \quad \text{on } (0, L) \times (t^n, t^{n+1}),
\tag{32}
$$

$$
\hat{u}_2(0, H, t) = \hat{u}_2(L, H, t) = 0, \quad \widehat{\boldsymbol{\sigma}}\widehat{\mathbf{n}}|_{\xi_1=0} = -\bar{p}(t)\hat{\mathbf{n}}, \quad \widehat{\boldsymbol{\sigma}}\widehat{\mathbf{n}}|_{\xi_1=L} = \mathbf{0},
\tag{33}
$$

and the initial conditions

$$
\hat{\mathbf{u}}(t^n) = \hat{\mathbf{u}}^n, \quad \hat{u}_2|_{\widehat{\Gamma}}(t^n) = \hat{u}_2^n|_{\widehat{\Gamma}}, \quad \eta(t^n) = \eta^n.
\tag{34}
$$

Then set

$$
\hat{\mathbf{u}}^{n+1/4} = \hat{\mathbf{u}}(t^{n+1}), \quad \hat{u}_2|_{\widehat{\Gamma}}^{n+1/4} = \hat{u}_2|_{\widehat{\Gamma}}(t^{n+1}), \quad \eta^{n+1/4} = \eta(t^{n+1}), \quad \hat{p}^{n+1} = \hat{p}(t^{n+1}).
$$

Step 2. The fluid advection.

Find $\hat{\mathbf{u}}$ and η such that

$$
\begin{cases}
\dfrac{\partial \hat{\mathbf{u}}}{\partial t} + \hat{\mathbf{u}}^{n+1/4} \cdot \nabla \hat{\mathbf{u}} = 0, \quad \text{in } \widehat{\Omega} \times (t^n, t^{n+1}) \\
\dfrac{\partial \eta}{\partial t}(\xi_1, t) = 0 \quad \text{on } (0, L) \times (t^n, t^{n+1}), \\
\varrho_s h_s \dfrac{\partial (\hat{u}_2|_{\widehat{\Gamma}})}{\partial t} = 0 \quad \text{on } (0, L) \times (t^n, t^{n+1}),
\end{cases}
\tag{35}
$$

with the boundary conditions:

$$
\begin{cases}
\hat{\mathbf{u}} = \hat{\mathbf{u}}^{n+1/4} \quad \text{on } \widehat{\Gamma}_-^{n+1/4} \times (t^n, t^{n+1}), \text{ where} \\
\widehat{\Gamma}_-^{n+1/4} = \{\mathbf{x} \in \mathbb{R}^2 | \mathbf{x} \in \partial\widehat{\Omega}, \, \hat{\mathbf{u}}^{n+1/4} \cdot \hat{\mathbf{n}} < 0\},
\end{cases}
\tag{36}
$$

and the initial conditions

$$
\hat{\mathbf{u}}(t^n) = \hat{\mathbf{u}}^{n+1/4}, \quad \hat{u}_2|_{\widehat{\Gamma}}(t^n) = \hat{u}_2|_{\widehat{\Gamma}}^{n+1/4}, \quad \eta(t^n) = \eta^{n+1/4}.
\tag{37}
$$

Then set

$$\hat{\mathbf{u}}^{n+2/4} = \hat{\mathbf{u}}(t^{n+1}), \quad \hat{u}_2|_{\widehat{\Gamma}}^{n+2/4} = \hat{u}_2|_{\widehat{\Gamma}}(t^{n+1}), \quad \eta^{n+2/4} = \eta(t^{n+1}).$$

Step 3. The ALE-advection.

Set $\mathbf{w}^{n+2/4} = -\dfrac{\xi_2}{H + \eta^n}\hat{u}_2^{n+2/4}|_{\widehat{\Gamma}}\mathbf{e}_2$, then find $\hat{\mathbf{u}}$ and η such that

$$\begin{cases} \dfrac{\partial \hat{\mathbf{u}}}{\partial t} + \mathbf{w}^{n+2/4} \cdot \nabla \hat{\mathbf{u}} = 0 & \text{in } \widehat{\Omega} \times (t^n, t^{n+1}) \\ \dfrac{\partial \eta}{\partial t}(\xi_1, t) = 0 & \text{on } (0, L) \times (t^n, t^{n+1}), \\ \varrho_s h_s \dfrac{\partial(\hat{u}_2|_{\widehat{\Gamma}})}{\partial t} = 0 & \text{on } (0, L) \times (t^n, t^{n+1}), \end{cases} \tag{38}$$

with the boundary conditions:

$$\begin{cases} \hat{\mathbf{u}} = \hat{\mathbf{u}}^{n+2/4} & \text{on } \widehat{\Gamma}_-^{n+2/4} \times (t^n, t^{n+1}) \text{ where} \\ \widehat{\Gamma}_-^{n+2/4} = \{\mathbf{x} \in \mathbb{R}^2 | \mathbf{x} \in \partial\widehat{\Omega}, \ \mathbf{w}^{n+2/4} \cdot \hat{\mathbf{n}} < 0\}, \end{cases} \tag{39}$$

and the initial conditions

$$\hat{\mathbf{u}}(t^n) = \hat{\mathbf{u}}^{n+2/4}, \quad \hat{u}_2|_{\widehat{\Gamma}}(t^n) = \hat{u}_2|_{\widehat{\Gamma}}^{n+2/4}, \quad \eta(t^n) = \eta^{n+2/4}. \tag{40}$$

Then set

$$\hat{\mathbf{u}}^{n+3/4} = \hat{\mathbf{u}}(t^{n+1}), \quad \hat{u}_2|_{\widehat{\Gamma}}^{n+3/4} = \hat{u}_2|_{\widehat{\Gamma}}(t^{n+1}), \quad \eta^{n+3/4} = \eta(t^{n+1}).$$

Step 4. Elastodynamics of the deformable boundary.

Find $\hat{\mathbf{u}}$ and η such that

$$\begin{cases} \dfrac{\partial \hat{\mathbf{u}}}{\partial t} = 0 & \text{in } \widehat{\Omega} \times (t^n, t^{n+1}), \\ \dfrac{\partial \eta}{\partial t}(\xi_1, t) = \hat{u}_2|_{\widehat{\Gamma}} & \text{in } (0, L) \times (t^n, t^{n+1}), \\ \varrho_s h_s \dfrac{\partial \hat{u}_2|_{\widehat{\Gamma}}}{\partial t} + C_0 \eta - C_1 \dfrac{\partial^2 \eta}{\partial x_1^2} = 0 & \text{in } (0, L) \times (t^n, t^{n+1}), \end{cases} \tag{41}$$

with the boundary conditions

$$\eta|_{\xi_1=0} = 0, \quad \eta|_{\xi_1=L} = 0, \tag{42}$$

and the initial conditions

$$\hat{\mathbf{u}}(t^n) = \hat{\mathbf{u}}^{n+3/4}, \quad \hat{u}_2|_{\widehat{\Gamma}}(t^n) = \hat{u}_2^{n+3/4}|_{\widehat{\Gamma}}, \quad \eta(t^n) = \eta^{n+3/4}. \tag{43}$$

Then set

$$\hat{\mathbf{u}}^{n+1} = \hat{\mathbf{u}}(t^{n+1}), \quad \hat{u}_2^{n+1}|_{\widehat{\Gamma}} = \hat{u}_2|_{\widehat{\Gamma}}(t^{n+1}), \quad \eta^{n+1} = \eta(t^{n+1}).$$

Do $t^n = t^{n+1}$ and return to Step 1.

Remark 1. Notice that in the first three steps we have $\partial\eta/\partial t = 0$. This means that we can update only the fluid velocity, keeping the location of the boundary fixed. On the other hand, in the last step, Step 4, we only update the position of the boundary and its velocity.

Remark 2. Even though the explicit evolution of the structure, calculated in Step 4, includes only the elastic part of the structure dynamics, the structure "feels" the fluid stress and the viscoelasticity through the initial condition for the velocity, namely $\hat{u}_2|_{\widehat{\Gamma}}(t^n)$. This is because $\hat{u}_2|_{\widehat{\Gamma}}(t^n)$ follows from the Stokes problem in Step 1 which embodies the fluid load to the structure as well as the structure viscoelasticity (see system (30)).

Remark 3. The most novel feature of the scheme is the way how the splitting is performed. Classical partitioned schemes separate fluid and structure in a different way. Firstly, the location of the structure and its velocity are assumed to be known and are used as Dirichlet data for the fluid solver. The solution of the fluid sub-problem provides the new fluid velocity and pressure from which the fluid stress on the structure is calculated. Secondly, the fluid stress is used as a load for the structure dynamics (elastic and/or viscoelastic). The structure solver provides the new position of the boundary and its velocity, and this is used as data for the next fluid step.

In the splitting approach presented in this article, the structure is split into its *hydrodynamic* part (structure load), the *viscoelastic* part, and the *elastic* part. The hydrodynamic part, consisting of the fluid stress on the boundary, and the viscoelastic part are treated together with the fluid equations (Step 1), while the purely elastic part is treated separately (Step 4). Throughout the entire scheme, fluid and structure are *coupled* through the kinematic lateral boundary condition. The fluid feels the presence of the structure through the initial and boundary conditions, while the structure feels the presence of the fluid through the initial condition for the velocity.

Moreover, since the calculation of the fluid velocity is separated from the calculation of the structure dynamics, we can use the already existing fluid and/or elastic solvers if we choose to do so. This modular nature of the scheme is one of its appealing features.

Remark 4. *Crucial* for the stability of the algorithm and the resolution of the *added mass effect* problem are the following four features of this scheme:

(1) the novel splitting of the structure equation;
(2) the treatment of the fluid load on the structure (with viscoelasticity) as a boundary condition for the Stokes problem in Step 1;
(3) the treatment of the hyperbolic part of the problem (fluid advection, ALE-advection and pure elasticity) in separate sub-problems;
(4) the treatment of the parabolic part of the problem (fluid viscosity and structure viscoelasticity) in one step (Step 1), contributing to the overall stability of the scheme.

See Section 6 for more details.

Remark 5. Another appealing feature of the scheme is that it is not necessary to calculate the fluid stress explicitly. As we shall see in Section (4.1) the coupling between the fluid stress and the structure dynamics in Step 1 is performed implicitly through the weak formulation thereby avoiding the calculation of the fluid stress all together.

Remark 6. In [2,45] a class of schemes was introduced to deal with the added mass effect by solving the fluid flow problem (and possibly the structure problem) using a Robin-type "transmission" condition. These transmission conditions are designed in an *ad hoc* manner by forming a linear combination of the two lateral boundary conditions (the dynamic and kinematic conditions) and the fluid stress on the structure needs to be calculated explicitly (the "Robin–Neumann" algorithm [2]). This is *not* the case with the kinematically coupled scheme presented in this paper. The transmission conditions follow naturally from the time-discretization of the full problem and the fluid stress on the structure is taken into account implicitly in Step 1. It needs to be mentioned, however, that the "Robin–Neumann" algorithm presented in [2] can be applied to both thick and thin structures, while the scheme introduced in the present article applies only to thin structures. Research leading to its generalization to the thick structure is under way.

Remark 7. The extension of our scheme to more realistic geometries does not add any conceptual difficulty. More precisely:

(1) The definition of the ALE-mapping and the domain velocity **w** will change. All the steps in the scheme will remain the same, except for the introduction of a new step, Step 5, where the new **w** is calculated;
(2) The model of the structure dynamics will be more complicated, written in curvilinear coordinates and, in some cases, including both longitudinal and transversal displacements. All the steps in our splitting scheme will remain the same, except that both the components of the fluid velocity will be non-zero at the boundary and equal to the structure velocity; the elasticity equations solved in Step 4 will be expressed in terms of the curvilinear coordinates and will have both the displacements as unknowns.

We conclude this section by summarizing the most appealing features of this scheme:

1. Elegant (natural) treatment of the added-mass effect avoiding the iterations between the fluid and the structure. See Remarks 4 and 6.
2. Modularity. See Remark 3.
3. Proper treatment of non-dissipative sub-steps. See Remark 4.
4. Fluid stress on the structure is taken into account implicitly thereby avoiding the need for an explicit calculation of the fluid stress at the boundary. See Remarks 5 and 6.

4. Treatment of the sub-problems

Due to the fact that the splitting is performed at the differential level, the scheme presented in the previous section is independent of the particular strategy that is chosen to solve each sub-problem. In particular, different time sub-steps

and different space discretizations can be used for the different sub-problems. Moreover, the communication between the sub-problems is limited to the initial and boundary conditions which makes it easy to incorporate the already written pieces of code as modules to solve each sub-problem.

Below, we describe the particular strategies that we advocate to solve each sub-problem. We took advantage of the modularity of the scheme by incorporating modules that we already developed for the solution of the incompressible Navier–Stokes equations defined on a fixed domain [31] and for free surface flows [28,30].

4.1. Step 1: the time-dependent Stokes sub-problem

In this sub-problem, the time-derivative of η over the interval (t^n, t^{n+1}) is zero and therefore $\eta(t) = \eta(t^n), \forall t \in (t^n, t^{n+1})$. This is the reason why we can safely map problem (30)–(33) back into the physical domain $\Omega(t^n)$ at time t^n. This leads to the following time-dependent Stokes problem:

$$\varrho_f \frac{\partial \mathbf{u}}{\partial t} = \nabla \cdot \boldsymbol{\sigma}, \quad \nabla \cdot \mathbf{u} = 0 \quad \text{in } \Omega(t^n) \times (t^n, t^{n+1}), \tag{44}$$

with the boundary conditions on $\Gamma(t^n)$:

$$u_1|_{\Gamma(t^n)} = 0$$
$$\varrho_s h_s \frac{\partial (u_2|_{\Gamma(t^n)})}{\partial t} + D_0 u_2|_{\Gamma(t^n)} - D_1 \frac{\partial^2 (u_2|_{\Gamma(t^n)})}{\partial x_1^2} = -\sqrt{1 + \left(\frac{\partial \eta^n}{\partial x_1}\right)^2} \boldsymbol{\sigma} \mathbf{n}|_{\Gamma(t^n)} \cdot \mathbf{e}_2, \tag{45}$$

with the symmetry boundary conditions at $x_2 = 0$:

$$\left.\frac{\partial u_1}{\partial x_2}\right|_{x_2=0} = 0, \quad u_2|_{x_2=0} = 0, \tag{46}$$

the inlet and outlet boundary conditions:

$$u_2(0, H, t) = u_2(L, H, t) = 0, \qquad \boldsymbol{\sigma}\mathbf{n}|_{x_1=0} = -\bar{p}(t)\mathbf{n}, \quad \boldsymbol{\sigma}\mathbf{n}|_{x_1=L} = \mathbf{0}, \tag{47}$$

and with the initial conditions

$$\mathbf{u}(t^n) = \mathbf{u}^n \quad \text{in} \quad \Omega(t^n), \quad u_2(t^n) = u_2^n \quad \text{on } \Gamma(t^n). \tag{48}$$

For the time-discretization of problem (44)–(48) we use a simple one step backward Euler scheme, while for the space discretization we use an isoparametric version of the Bercovier–Pironneau finite-elements spaces. This finite element approximation, introduced in [6] and further discussed in [27,28,30], is also known as $P1 - iso - P2$ and $P1$ approximation. Its main advantage is the increased accuracy in the treatment of the non-polygonal portions of the boundary. A careful treatment of the boundary is very important for the problem at hand, since the coupling between the fluid flow and the structure dynamics takes place on a portion of the domain boundary.

To enforce the incompressibility of the velocity field and to obtain the related pressure we use a preconditioned conjugate gradient method (see e.g. [27]). We emphasize that several preconditioners have been developed for the classical case of Dirichlet and/or stress related boundary conditions, but no preconditioner was available for the particular boundary condition given in (45). In order to fill this gap, the first two authors developed a new preconditioner for this problem, presented and justified in [29]. The new preconditioner operates in the pressure space and it reduces substantially the number of iterations when compared to a conjugate gradient algorithm equipped with the canonical scalar product of L^2. For the sake of completeness, we describe this new preconditioned conjugate gradient algorithm below.

We begin by writing the variational formulation of the time-discretized problem. Let $V(t)$ denote the following function space:

$$V(t) = \left\{\mathbf{v} \in (H^1(\Omega(t)))^2 : v_2|_{x_2=0} = 0, v_1|_{\Gamma(t)} = 0, v_2|_{\Gamma(t)} \in H_0^1(\Gamma(t))\right\}.$$

As in Step 1, let us denote by $\mathbf{u}^n$ and p^n the solution at $t = t^n$. Then the variational formulation of the time-discretized problem (44)–(48) can be written as follows: Find $\mathbf{u}^{n+1/4} \in V(t^n)$ and $p^{n+1/4} \in L^2(\Omega(t^n))$ such that

$$\frac{\varrho_f}{\Delta t} \int_{\Omega(t^n)} \mathbf{u}^{n+1/4} \cdot \mathbf{v} d\mathbf{x} + \frac{\varrho_s h_s}{\Delta t} \int_0^L u_2^{n+1/4}|_{\Gamma(t^n)} v_2|_{\Gamma(t^n)} dx_1 + 2\mu \int_{\Omega(t^n)} \mathbf{D}(\mathbf{u}^{n+1/4}) : \mathbf{D}(\mathbf{v}) d\mathbf{x}$$
$$+ D_1 \int_0^L \frac{\partial (u_2^{n+1/4}|_{\Gamma(t^n)})}{\partial x_1} \frac{\partial (v_2|_{\Gamma(t^n)})}{\partial x_1} dx_1 + D_0 \int_0^L u_2^{n+1/4}|_{\Gamma(t^n)} v_2|_{\Gamma(t^n)} dx_1 - \int_{\Omega(t^n)} p^{n+1/4} \nabla \cdot \mathbf{v} d\mathbf{x} = L(\mathbf{v}), \quad \forall \mathbf{v} \in V(t^n), \tag{49}$$

and

$$\int_{\Omega(t^n)} q \nabla \cdot \mathbf{u}^{n+1/4} d\mathbf{x} = 0, \quad \forall q \in L^2(\Omega(t^n)),$$

where

$$L(\mathbf{v}) = \frac{\varrho_f}{\Delta t} \int_{\Omega(t^n)} \mathbf{u}^n \cdot \mathbf{v} \, d\mathbf{x} + \frac{\varrho_s h_s}{\Delta t} \int_0^L u_2^n|_{\Gamma(t^n)} v_2|_{\Gamma(t^n)} dx_1 + \int_0^H \bar{p}(t^{n+1}) v_1|_{x_1=0} dx_2.$$

Let $\alpha = \varrho_f/\Delta t$ and $\beta = \varrho_s h_s/\Delta t + D_0$ (for the details about the choice of these parameters see [29]). Our preconditioned conjugate gradient algorithm for the solution of the above generalized Stokes problem reads as follows:

Take an initial guess $p^0 \in L^2(\Omega(t^n))$ and find $\mathbf{u}^0 \in V(t^n)$ such that $\forall \mathbf{v} \in V(t^n)$ it holds

$$\alpha \int_{\Omega(t^n)} \mathbf{u}^0 \cdot \mathbf{v} d\mathbf{x} + \beta \int_0^L u_2^0|_{\Gamma(t^n)} v_2|_{\Gamma(t^n)} dx_1 + 2\mu \int_{\Omega(t^n)} \mathbf{D}(\mathbf{u}^0) : \mathbf{D}(\mathbf{v}) d\mathbf{x} + D_1 \int_0^L \frac{\partial(u_2^0|_{\Gamma(t^n)})}{\partial x_1} \frac{\partial(v_2|_{\Gamma(t^n)})}{\partial x_1} dx_1$$
$$= \int_{\Omega(t^n)} p^0 \nabla \cdot \mathbf{v} d\mathbf{x} + L(\mathbf{v}), \tag{50}$$

and set $r^0 = \nabla \cdot \mathbf{u}^0$.

Solve now

$$\begin{cases} -\Delta\varphi^0 = r^0 & \text{in } \Omega(t^n) \\ \varphi^0|_{x_1=0} = 0, \quad \varphi^0|_{x_1=L} = 0, \\ \left.\frac{\partial\varphi^0}{\partial n}\right|_{x_2=0} = 0, \quad \varphi^0|_{\Gamma(t^n)} + \frac{\beta}{\alpha}\left.\frac{\partial\varphi^0}{\partial n}\right|_{\Gamma(t^n)} = 0. \end{cases} \tag{51}$$

Then set $g^0 = \mu r^0 + \alpha\varphi^0, w^0 = g^0$.

For $k \geq 0$, assuming that p^k, r^k, g^k, w^k are known, compute $p^{k+1}, r^{k+1}, g^{k+1}, w^{k+1}$ as follows:

First find $\bar{\mathbf{u}}^k \in V(t^n)$ such that $\forall \mathbf{v} \in V(t^n)$ it holds

$$\alpha \int_{\Omega(t^n)} \bar{\mathbf{u}}^k \cdot \mathbf{v} d\mathbf{x} + \beta \int_0^L \bar{u}_2^k|_{\Gamma(t^n)} v_2|_{\Gamma(t^n)} dx_1 + 2\mu \int_{\Omega(t^n)} \mathbf{D}(\bar{\mathbf{u}}^k) : \mathbf{D}(\mathbf{v}) d\mathbf{x} + D_1 \int_0^L \frac{\partial(\bar{u}_2^k|_{\Gamma(t^n)})}{\partial x_1} \frac{\partial(v_2|_{\Gamma(t^n)})}{\partial x_1} dx_1 = \int_{\Omega(t^n)} w^k \nabla \cdot \mathbf{v} d\mathbf{x}, \tag{52}$$

and set $\bar{r}^k = \nabla \cdot \bar{\mathbf{u}}^k$.

Compute

$$\varrho_k = \int_{\Omega(t^n)} r^k g^k d\mathbf{x} / \int_{\Omega(t^n)} \bar{r}^k w^k d\mathbf{x}, \tag{53}$$

and update p^k and r^k via $p^{k+1} = p^k - \varrho_k w^k, r^{k+1} = r^k - \varrho_k \bar{r}^k$.

Next find $\bar{\varphi}^k$ such that

$$\begin{cases} -\Delta\bar{\varphi}^k = \bar{r}^k & \text{in } \Omega(t^n) \\ \bar{\varphi}^k|_{x_1=0} = 0, \quad \bar{\varphi}_{x_1=L}^k = 0, \\ \left.\frac{\partial\bar{\varphi}^k}{\partial n}\right|_{x_2=0} = 0, \quad \bar{\varphi}^k|_{\Gamma(t^n)} + \frac{\beta}{\alpha}\left.\frac{\partial\bar{\varphi}^k}{\partial n}\right|_{\Gamma(t^n)} = 0. \end{cases} \tag{54}$$

Then update g^k via $g^{k+1} = g^k - \varrho_k(\mu\bar{r}^k + \alpha\bar{\varphi}^k)$.

If

$$\int_{\Omega(t^n)} r^{k+1} g^{k+1} d\mathbf{x} / \int_{\Omega(t^n)} r^0 g^0 d\mathbf{x} \leqslant \epsilon, \tag{55}$$

take $p = p^{k+1}$; else, compute

$$\gamma_k = \int_{\Omega(t^n)} r^{k+1} g^{k+1} d\mathbf{x} / \int_{\Omega(t^n)} r^k g^k d\mathbf{x}, \tag{56}$$

and update w^k via $w^{k+1} = g^{k+1} + \gamma_k w^k$.

Do $k = k + 1$ and return to (52).

The vectors g^k and w^k that appear in scheme above are classical quantities encountered in all conjugate gradient algorithms (see, e.g. [27], Chapter 3). Both are residuals whose norm measures a distance to the solution we are looking for; we use them to improve the approximate solution they are associated with, in order to guarantee the convergence of the algorithm. For the problem under consideration, g^k and w^k are nothing but pressure corrections since the conjugate gradient algorithm discussed here is a pressure driven method to solve a new (to the best of our knowledge) kind of Stokes problem.

The main novelty of the scheme (50)–(56) lies in the design of new boundary conditions for the auxiliary function φ, satisfied on the deformable portion of the boundary. From the classical theory for preconditioned conjugate gradient methods for incompressible viscous fluids, see [27] and the references therein, Dirichlet boundary conditions for the normal compo-

nent of the velocity imply $\partial \varphi / \partial n = 0$ for the auxiliary function. On the other hand, the portion of the boundary where a condition on the fluid stress is imposed invokes $\varphi = 0$ for the auxiliary function. For the boundary conditions of the problem at hand, it was shown in [29] that a Robin-type boundary condition in problems (51) and (54) is the condition to be imposed on the auxiliary function φ at the deformable portion of the boundary. Moreover, it was shown that the optimal constant in the Robin condition for the auxiliary function φ is β/α, which equals the ratio $\varrho_s h_s/\varrho_f$ when the viscoelastic constant D_0 is zero.

Remark 8. It is interesting to notice that the same ratio $\varrho_s h_s/\varrho_f$ appears as the critical parameter value in the stability analysis related to the added mass effect observed in the explicit schemes, as reported in [11].

Remark 9. The use of a preconditioner in the pressure space requires the solution of the elliptic problem (54) at each iteration of the conjugate gradient calculation. Moreover, this elliptic problem is defined on the domain $\Omega(t^n)$ which changes at each time step and therefore the stiffness matrix of the elliptic problem should be recalculated at each time step. In order to avoid this, we assemble the stiffness matrix on the initial domain and we "freeze" it, using the same matrix at every time step, even if the geometry of the domain has changed. By doing this, we need to assemble the stiffness matrix only once and this still gives excellent numerical results, as shown in Section 5.

4.2. The non-dissipative steps: fluid advection, ALE-advection and elasticity

Steps 2–4 where we solve for the fluid advection (35) and (36), the advection due to the ALE-description of the domain deformation (38) and (39), and the purely elastic structure problem (41) and (42), respectively, are all non-dissipative transport problems. In an attempt to preserve this feature of the problem, it is natural to use solvers with low numerical dissipation. Notice that thanks to the operator splitting approach, the time steps used in Steps 2–4, can be much smaller than that used in Step 1. More details are presented next.

Step 2: In order to solve the advection step (35)–(37), we use a wave-like equation method [27,31,46]. This approach preserves the hyperbolic nature of advection, it introduces low numerical dissipation and it is easily implemented. In particular, we use here a second-order accurate time-discretization scheme which is discussed, e.g. in [27], Chapter 6, and in [46].

Step 3: In order to solve the transport problem (38)–(40) we again use the wave-like equation approach. Due to the fact that in our problem $w_1 = 0$, equation (38) does not contain x_1 differentiation of $\hat{\mathbf{u}}$ and therefore the problem reduces to the solution of a family (infinite for the continuous problem, finite for the discrete ones) of transport problems in one space dimension along the vertical direction. Then for $\xi_1 \in (0,L)$, each component of $\hat{\mathbf{u}}$ is a solution of a transport problem of the following form:

$$\begin{cases} \dfrac{\partial \varphi}{\partial t} - a\xi_2 \dfrac{\partial \varphi}{\partial \xi_2} = 0 & \text{on } (0,H) \times (t^n, t^{n+1}), \\ \varphi(t^n) = \varphi_0, \\ \varphi(H,t) = b & \text{in } (t^n, t^{n+1}): \quad \text{if } a > 0, \end{cases} \tag{57}$$

where a and b are constant with respect to ξ_2 and t. The solution of this problem is discussed in [28,30].

Step 4: Problem (41)–(43) captures the contribution from the purely elastic part of the structure equation, without any load. System (41) can be rewritten as the following wave equation:

$$\varrho_s h_s \dfrac{\partial^2 \eta}{\partial t^2} + C_0 \eta - C_1 \dfrac{\partial^2 \eta}{\partial x_1^2} = 0 \quad \text{on } (0,L) \times (t^n, t^{n+1}) \tag{58}$$

which we solve using a second-order finite difference scheme such as the one described in [27], Section 31.5.4.3.

5. Numerical results

We present here some numerical results with the goal of testing the performance of the kinematically coupled scheme proposed in this article.

We consider the test case proposed by Formaggia et al. in [25], which has now become a standard in testing fluid–structure interaction techniques for blood flow applications, see e.g. [2,3,32,45]. This benchmark problem corresponds to the problem presented in Section (2) with the viscoelastic coefficient $D_0 = 0$. The flow is driven by the time-dependent pressure data

$$\bar{p}(0, x_2, t) = \begin{cases} \dfrac{p_{max}}{2} \left[1 - \cos\left(\dfrac{2\pi t}{t_{max}}\right) \right] & \text{if } t \leqslant t_{max}, \\ 0 & \text{if } t > t_{max} \end{cases} \tag{59}$$

Table 1
Geometry, fluid and structure parameters.

| Geometry				Structure Parameters			
Length	L	6	cm	Young's modulus	E	0.75×10^6	dynes/cm^2
Height	H	0.5	cm	Poisson's ratio	v	0.5	[1]
Fluid parameters				Density	ρ_s	1.1	g/cm^3
Viscosity	μ	0.035	poise	Thickness	h_s	0.1	cm
Density	ρ_f	1	g/cm^3	Viscoelasticity	D_1	0.01	poise cm

where $p_{max} = 2 \times 10^4$ (dynes/cm^2) and $t_{max} = 0.005$ (s). The elastic constants in (6) are given by $C_0 = Eh_s/H^2(1 - v^2)$ and $C_1 = Eh_s/2(1 + v)$, where E is the Young's modulus and v is the Poisson's ratio. The geometrical and physical parameters of the problem are specified in Table 1.

The numerical solution of this benchmark problem obtained with the kinematically coupled scheme is shown in Fig. 3. We show the solution at six different snap-shots. Each snapshot contains information about the pressure (colormap), velocity (streamlines) and structure displacement (solid contour of the fluid domain). The results show a forward moving pressure wave, with positive flow rate, which reaches the end of the domain and gets reflected. The reflected wave is characterized by negative values of the pressure and positive flow rates [12,25]. The results obtained with the kinematically coupled scheme are in excellent agreement with those obtained in [25] using an implicit scheme.

Results in Fig. 3 have been obtained with $\Delta t = 5 \times 10^{-5}$. A smaller time step of $\Delta t/5$ has been used in the non-dissipative sub-problems, namely for the fluid advection (35)–(37), the ALE-advection (38)–(40) and the elastodynamics sub-problem (41)–(43). The domain was discretized using uniform triangular structured meshes for pressure and velocity defined on the rectangular reference domain $\widehat{\Omega}$, with the mesh sizes $h_p = H/8$ and $h_v = h_p/2$, respectively. The pressure mesh and the velocity mesh are then deformed according to the ALE-mapping defined in (11). Fig. 4 (top) shows the velocity mesh for the physical flow region at time $t = 12$ (ms), with a magnified view of the most deformed area shown at the bottom of the same figure.
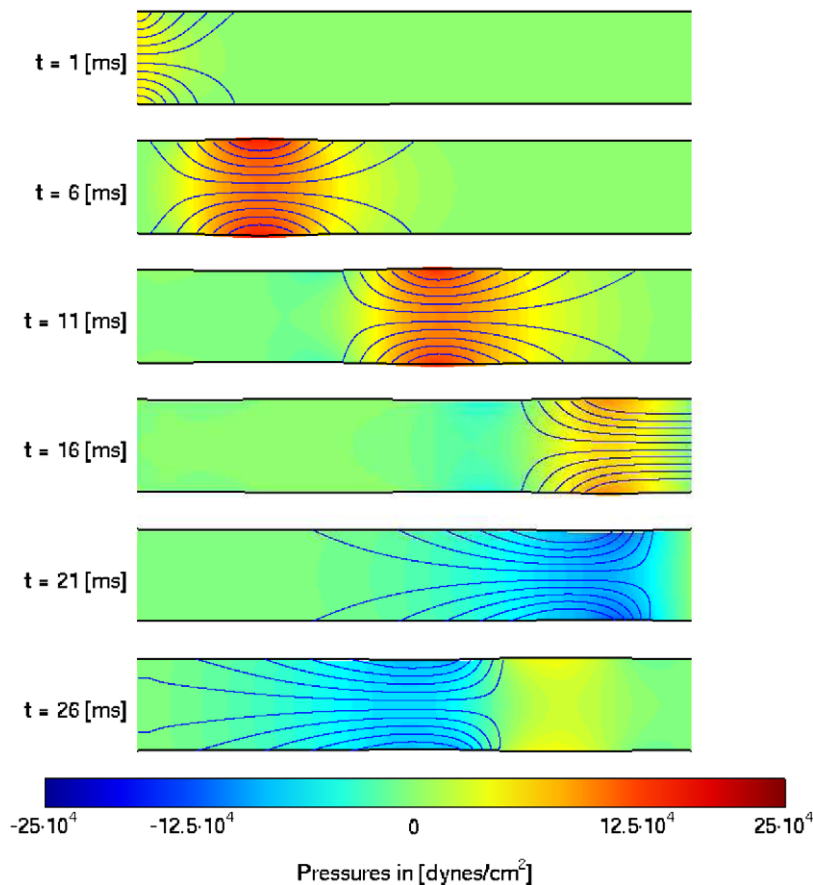
Fig. 3. Snap-shots of the numerical solution of (30)–(42) containing information on pressure (colormap), velocity (streamlines) and structure displacement (solid contour of the flow region). (For interpretation of the references to colour in this figure legend, the reader is referred to the web version of this article.)
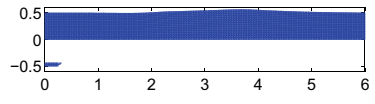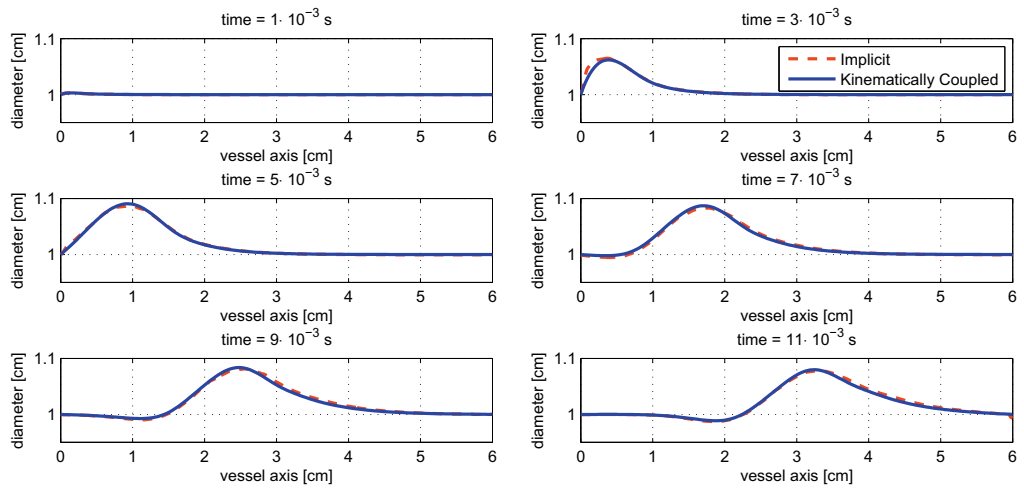
p [dynes/cm^2]

time = 7· 10^{-3} s

vessel axis [cm]

Fig. 7. Diameter of the vessel computed with the kinematically coupled scheme with $\Delta t = 5 \times 10^{-5}$ (*solid line*) and with the implicit algorithm used by Nobile in [44] with $\Delta t = 10^{-4}$ (*dashed line*).

Figs. 5–7 show a comparison between the numerical solutions to problem (3)–(10) obtained with our kinematically coupled scheme (30)–(43) (solid line) and with the implicit scheme used by Nobile in [44] (dashed line). The results show an excellent agreement between the computed average pressure, shown in Fig. 5, the flow rate, shown in Fig. 6, and the vessel diameter, shown in Fig. 7, at six different times. It is interesting to notice that the time steps used for the kinematically coupled scheme and for the implicit scheme are of the same order of magnitude. More precisely, a time step of $\Delta t = 1 \times 10^{-4}$ was used for the implicit scheme, while a time step of $\Delta t = 5 \times 10^{-5}$ was used for the kinematically coupled scheme. We remark again that no iterations between fluid and structure are necessary for the calculation of the solution using the kinematically coupled scheme. This is in contrast with implicit schemes that are much more computationally expensive since they require solving a sequence of nonlinear, strongly coupled problems using, e.g. fixed point and Newton's methods, or Steklov–Poincaré-based domain decomposition methods.

The kinematically coupled scheme presented in this article has been obtained using a Lie's time-splitting scheme, which is known to be first-order accurate in time. This is confirmed by the results shown in Fig. 8. Here we used a domain triangulation of size $h_p = H/8$ for the pressure and $h_v = h_p/2$ for the velocity, and we ran the simulations using
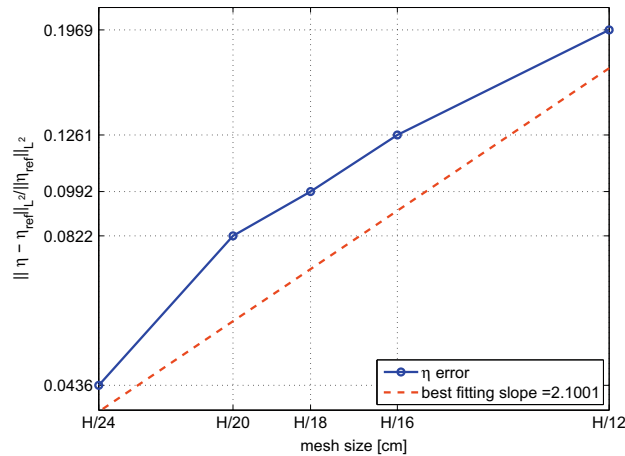
Table 2
Convergence in time of the kinematically coupled scheme (mesh size $h_p = H/8$).

Δt (s)	$\frac{\|p-p_{ref}\|_{l2}}{\|p_{ref}\|_{l2}}$	L_2 order	$\frac{\|\mathbf{u}-\mathbf{u}_{ref}\|_{l2}}{\|\mathbf{u}_{ref}\|_{l2}}$	L_2 order	$\frac{\|\eta-\eta_{ref}\|_{l2}}{\|\eta_{ref}\|_{l2}}$	L_2 order
1×10^{-4}	1.310×10^{-2}	–	1.088×10^{-2}	–	5.918×10^{-2}	–
5×10^{-5}	7.818×10^{-3}	0.7443	5.967×10^{-3}	0.8664	3.513×10^{-2}	0.7526
1×10^{-5}	1.700×10^{-3}	0.9482	1.327×10^{-3}	0.9339	7.589×10^{-3}	0.9521
5×10^{-6}	7.724×10^{-4}	1.1376	6.166×10^{-4}	1.1063	3.446×10^{-3}	1.1390
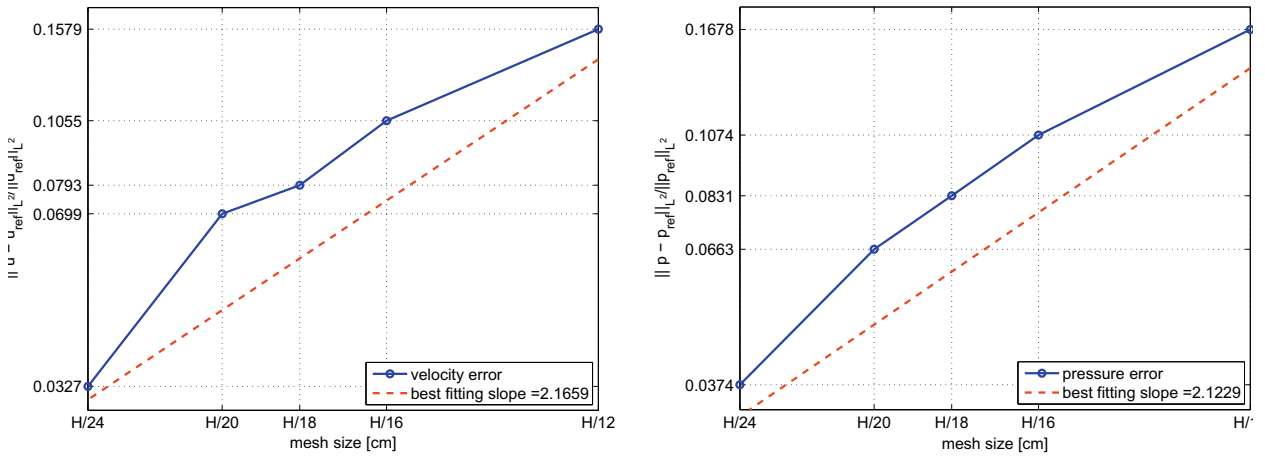
(a) Velocity: spatial convergence.

(b) Pressure: spatial convergence.

(c) Structure displacement: spatial convergence.

Fig. 9. The figures show second-order accuracy in space of the kinematically coupled scheme.

Table 3
Convergence in space for the kinematically coupled scheme (time step $\Delta t = 5 \times 10^{-6}$).

Mesh size	$\frac{\|p-p_{ref}\|_{l^2}}{\|p_{ref}\|_{l^2}}$	L_2 order	$\frac{\|\mathbf{u}-\mathbf{u}_{ref}\|_{l^2}}{\|\mathbf{u}_{ref}\|_{l^2}}$	L_2 order	$\frac{\|\eta-\eta_{ref}\|_{l^2}}{\|\eta_{ref}\|_{l^2}}$	L_2 order
$H/12$	1.678×10^{-1}	–	1.579×10^{-1}	–	1.969×10^{-1}	–
$H/16$	1.074×10^{-1}	1.5500	1.055×10^{-1}	1.4024	1.261×10^{-1}	1.5475
$H/18$	0.831×10^{-1}	2.1794	0.793×10^{-1}	2.4180	0.992×10^{-1}	2.0372
$H/20$	0.663×10^{-1}	2.1494	0.699×10^{-1}	1.1933	0.822×10^{-1}	1.7838
$H/24$	0.374×10^{-1}	3.1395	0.327×10^{-1}	4.1757	0.436×10^{-1}	3.4751

$\Delta t = 1 \times 10^{-4}, 5 \times 10^{-5}, 1 \times 10^{-5}, 5 \times 10^{-6}$, and 1×10^{-6}. Results obtained with the different time steps are then compared with a reference solution, which was taken to be the one obtained with $\Delta t = 10^{-6}$. Numerical values for the L^2-errors are reported in Table 2.

In Fig. 9, we show the rate of convergence of the kinematically coupled scheme as we vary the mesh size. Here we consider $\Delta t = 5 \times 10^{-6}$ and we run simulations using $h_p = H/6, H/8, H/9, H/10, H/12$ and $H/16$ as mesh sizes for the pressure mesh. The reference solution was taken to be the one obtained with $h_p = H/16$. Results in Fig. 9 suggest a spatial rate of convergence of the order of 2. Numerical values for L^2-errors are reported in Table 3.

6. On the stability of the kinematically coupled scheme

In this section we discuss the stability properties of the kinematically coupled scheme (30)–(43). The stability analysis will be performed on a simplified problem which still retains the main difficulties associated with the "added-mass" effect, as shown in [11]. This problem consists of the flow of an incompressible viscous fluid in a two-dimensional channel with thin deformable walls assuming that: (1) the Reynolds number is small enough to justify the use of the Stokes equations for the fluid flow; (2) the displacement of the deformable portion of the boundary is small enough to be neglected. Under these assumptions, the geometry of the fluid domain is fixed and problem (3)–(10) reads as follows:

$$\varrho_f \frac{\partial \mathbf{u}}{\partial t} = \nabla \cdot \boldsymbol{\sigma}, \quad \nabla \cdot \mathbf{u} = 0 \quad \text{in } \Omega \text{ for } t \in (0, T), \tag{60}$$

where Ω is the rectangular domain $\Omega = (0, L) \times (0, H)$. At the inlet and outlet sections we impose the same stress conditions as in (4), and at the bottom boundary we impose the same symmetry conditions as in Eq. (5). The deformable portion of the domain boundary is now the straight line

$$\Gamma = \{(x_1, x_2) \in \mathbb{R}^2 | x_1 \in (0, L), x_2 = H\}, \tag{61}$$

and the dynamic and kinematic coupling conditions on Γ now read as follows:

$$\varrho_s h_s \frac{\partial^2 \eta}{\partial t^2} + C_0 \eta - C_1 \frac{\partial^2 \eta}{\partial x_1^2} + D_0 \frac{\partial \eta}{\partial t} - D_1 \frac{\partial^3 \eta}{\partial t \partial x_1^2} = -\boldsymbol{\sigma} \mathbf{n} \cdot \mathbf{e}_2 \quad \text{on } \Gamma \times (0, T), \tag{62}$$

$$u_1 = 0, \quad u_2 = \frac{\partial \eta}{\partial t} \quad \text{on } \Gamma \times (0, T), \tag{63}$$

where $\mathbf{e}_2 = (0, 1)$. The problem is completed by the boundary conditions (9) for η, and the initial conditions (10) for $\mathbf{u}, \eta$ and $\partial \eta / \partial t$. Defining

$$V = \left\{ \mathbf{v} \in (H^1(\Omega))^2 : v_2|_{x_2=0} = 0, v_1|_\Gamma = 0, v_2 \in H_0^1(\Gamma) \right\},$$

a weak formulation of the problem is given by: For $t \in (0, T)$, find $\mathbf{u} \in V, p \in L^2(\Omega)$ and $\eta \in H_0^1(0, L)$ such that

$$\varrho_f \int_\Omega \frac{\partial \mathbf{u}}{\partial t} \cdot \mathbf{v} \, d\mathbf{x} + 2\mu \int_\Omega \mathbf{D}(\mathbf{u}) : \mathbf{D}(\mathbf{v}) \, d\mathbf{x} - \int_\Omega p \nabla \cdot \mathbf{v} \, d\mathbf{x} + \int_0^L \left(\varrho_s h_s \frac{\partial^2 \eta}{\partial t^2} + C_0 \eta + D_0 \frac{\partial \eta}{\partial t} \right) v_2|_\Gamma \, dx_1$$

$$+ \int_0^L \left(C_1 \frac{\partial \eta}{\partial x_1} + D_1 \frac{\partial^2 \eta}{\partial t \partial x_1} \right) \frac{\partial (v_2|_\Gamma)}{\partial x_1} \, dx_1 = \int_0^H \bar{p}(t) v_1|_{x_1=0} dx_2, \quad \forall \mathbf{v} \in V. \tag{64}$$

By taking $\mathbf{u}$ as test function, it is easy to see that the solution of problem (64) satisfy the energy identity:

$$\frac{1}{2} \frac{d}{dt} \mathcal{E} + \mathcal{D} = \mathcal{F} \quad \text{for } t \in (0, T), \tag{65}$$

where $\mathcal{E}$ represents the energy of the system, $\mathcal{D}$ represents the dissipation in the system, and $\mathcal{F}$ represents the action of the external forces. More precisely, the energy $\mathcal{E}$ is given by the sum of the kinetic and elastic energy:

$$\mathcal{E} = \varrho_f \|\mathbf{u}\|_{L^2(\Omega)}^2 + \varrho_s h_s \left\| \frac{\partial \eta}{\partial t} \right\|_{L^2(0,L)}^2 + C_0 \|\eta\|_{L^2(0,L)}^2 + C_1 \left\| \frac{\partial \eta}{\partial x_1} \right\|_{L^2(0,L)}^2, \tag{66}$$

the term $\mathcal{D}$ includes the dissipation due to the fluid viscosity and the structure viscoelasticity:

$$\mathcal{D} = 2\mu \|\mathbf{D}(\mathbf{u})\|_{L^2(\Omega)}^2 + D_0 \left\|\frac{\partial \eta}{\partial t}\right\|_{L^2(0,L)}^2 + D_1 \left\|\frac{\partial^2 \eta}{\partial t \partial x_1}\right\|_{L^2(0,L)}^2, \tag{67}$$

while the term $\mathcal{F}$ includes the action of the given stress imposed at the inlet:

$$\mathcal{F} = \int_0^H \bar{p}(t) v_1|_{x_1=0} \, dx_2. \tag{68}$$

It is important to emphasize the key role played by the dynamic and kinematic conditions in the derivation of the energy identity (65). The dynamic condition allowed to write an integral equation involving simultaneously fluid and structure, see (64), while the kinematic condition allowed to obtain positive terms for the energy, see (66), and for the dissipation in the structure, see (67). It is worth to notice how the mass of the structure multiplies a positive term which represents the structure contribution to the kinetic energy of the system and, in some sense, it is as if the fluid had an "added-mass" on the boundary. This "added-mass" does not present any issue at the continuous level, but problems may arise at the discrete level if the coupling conditions are not properly handled. In particular, when the kinematic condition is treated explicitly, as in the traditional partitioned schemes, a mismatch is introduced between fluid and structure velocities at the boundary and, as a consequence, the mass of the structure multiplies a term which may change sign depending on the parameters of the problem. More precisely, it has been proved in [11] that traditional partitioned schemes are unconditionally unstable whenever $\varrho_s h_s / \varrho_f \leqslant 1$, which is the case in blood flow simulations. The improper treatment of the kinematic condition is therefore one of the main sources of instability of the traditional splitting schemes because it effectively causes the "mass" on the boundary to be "subtracted" instead of "added", compromising the energy balance at the discrete level.

The main rationale behind our splitting strategy is to enforce the kinematic condition in a strong way in order to ensure a proper matching between the fluid and structure velocities at the boundary in each sub-step of our scheme. The design of our splitting scheme is mainly guided by the energy identity (65) and our main goal is to ensure that, at the discrete level, the structure velocity gives a positive contribution to the energy of the system. To make our point more precise, let us write the algorithm resulting from the application of the kinematically coupled scheme to problem (60)–(63). The algorithm consists of the following two steps:

Step 1. The Stokes problem with the given inlet stress, the structure viscoelasticity and the fluid stress exerted on the structure.

Find $\mathbf{u}, p$ and η such that

$$\varrho_f \frac{\partial \mathbf{u}}{\partial t} = \nabla \cdot \boldsymbol{\sigma}, \quad \nabla \cdot \mathbf{u} = 0 \quad \text{in } \Omega \times (t^n, t^{n+1}), \tag{69}$$

with the boundary conditions:

$$u_1|_\Gamma = 0, \quad \varrho_s h_s \frac{\partial (u_2|_\Gamma)}{\partial t} + D_0 u_2|_\Gamma - D_1 \frac{\partial^2 (u_2|_\Gamma)}{\partial x_1^2} = -\boldsymbol{\sigma} \mathbf{n}|_\Gamma \cdot \mathbf{e}_2, \tag{70}$$

$$\left.\frac{\partial u_1}{\partial x_2}\right|_{x_2=0} = 0, \quad u_2|_{x_2=0} = 0, \tag{71}$$

$$u_2(0, H, t) = u_2(L, H, t) = 0, \quad \boldsymbol{\sigma} \mathbf{n}|_{x_1=0} = -\bar{p}(t)\mathbf{n}, \quad \boldsymbol{\sigma} \mathbf{n}|_{x_1=L} = \mathbf{0}, \tag{72}$$

and the initial conditions

$$\mathbf{u}(t^n) = \mathbf{u}^n \quad \text{in } \Omega, \quad u_2(t^n) = u_2^n \quad \text{on } \Gamma. \tag{73}$$

Then set

$$\mathbf{u}^{n+1/2} = \mathbf{u}(t^{n+1}), \quad u_2^{n+1/2}|_\Gamma = u_2|_\Gamma(t^{n+1}), \quad p^{n+1} = p(t^{n+1}), \quad \eta^{n+1/2} = \eta(t^{n+1}).$$

Step 2. Elastodynamics of the deformable boundary.

Find $\mathbf{u}$ and η such that

$$\frac{\partial \mathbf{u}}{\partial t} = 0 \quad \text{in } \Omega \times (t^n, t^{n+1}), \tag{74}$$

$$\frac{\partial \eta}{\partial t}(x_1, t) = u_2|_\Gamma \quad \text{in } (0, L) \times (t^n, t^{n+1}), \tag{75}$$

$$\varrho_s h_s \frac{\partial u_2|_\Gamma}{\partial t} + C_0 \eta - C_1 \frac{\partial^2 \eta}{\partial x_1^2} = 0 \quad \text{in } (0, L) \times (t^n, t^{n+1}), \tag{76}$$

with the boundary conditions

$$\eta|_{x_1=0} = 0, \quad \eta|_{x_1=L} = 0, \tag{77}$$

and the initial conditions

$$\mathbf{u}(t^n) = \mathbf{u}^{n+1/2}, \quad u_2|_\Gamma(t^n) = u_2^{n+1/2}|_\Gamma, \quad \eta(t^n) = \eta^{n+1/2}. \tag{78}$$

Then set

$$\mathbf{u}^{n+1} = \mathbf{u}(t^{n+1}), \quad u_2^{n+1}|_\Gamma = u_2|_\Gamma(t^{n+1}), \quad \eta^{n+1} = \eta(t^{n+1}).$$

Do $t^n = t^{n+1}$ and return to Step 1.

Solution of the problem in Step 1 satisfies the following identity:

$$\frac{1}{2}\frac{d}{dt}\mathcal{E}_I + \mathcal{D}_I = \mathcal{F}_I \quad \text{for } t \in (t^n, t^{n+1}), \tag{79}$$

wherewhere

$$\mathcal{E}_I = \varrho_f \|\mathbf{u}\|_{L^2(\Omega)}^2 + \varrho_s h_s \|u_2\|_{L^2(\Gamma)}^2, \tag{80}$$

$$\mathcal{D}_I = 2\mu \|\mathbf{D}(\mathbf{u})\|_{L^2(\Omega)}^2 + D_0 \|u_2\|_{L^2(\Gamma)}^2 + D_1 \left\|\frac{\partial u_2}{\partial x_1}\right\|_{L^2(\Gamma)}^2, \tag{81}$$

$$\mathcal{F}_I = \int_0^H \bar{p}(t^{n+1})u_1|_{x_1=0}\, dx_2. \tag{82}$$

Let us now see how this energy identity looks at the time-discrete level. As discussed in Section 4, we use a backward Euler scheme for the time-discretization of Step 1 and we achieve a weak formulation of the time-discrete problem similar to (49). By taking $\mathbf{u}^{n+1/2}$ as test function, we obtain the following identity:

$$\frac{\varrho_f}{\Delta t}\|\mathbf{u}^{n+1/2}\|_{L^2(\Omega)}^2 + \left(\frac{\varrho_s h_s}{\Delta t} + D_0\right)\left\|u_2^{n+1/2}\right\|_{L^2(\Gamma)}^2 + 2\mu\|\mathbf{D}(\mathbf{u}^{n+1/2})\|_{L^2(\Omega)}^2 + D_1\left\|\frac{\partial u_2^{n+1/2}}{\partial x_1}\right\|_{L^2(\Gamma)}^2$$

$$= \frac{\varrho_f}{\Delta t}\int_\Omega \mathbf{u}^n \cdot \mathbf{u}^{n+1/2}\, d\mathbf{x} + \frac{\varrho_s h_s}{\Delta t}\int_0^L u_2|_\Gamma^n u_2|_\Gamma^{n+1/2}\, dx_1 + \int_0^H \bar{p}(t^{n+1})u_1|_{x_1=0}^{n+1/2}dx_2, \tag{83}$$

where $\Delta t = t^{n+1} - t^n$. Now we proceed with the estimates of the right hand side of Eq. (83). Using Young's inequality we get

$$\frac{\varrho_f}{\Delta t}\int_\Omega \mathbf{u}^n \cdot \mathbf{u}^{n+1/2}\, d\mathbf{x} \leqslant \frac{\varrho_f}{2\Delta t}\|\mathbf{u}^n\|_{L^2(\Omega)}^2 + \frac{\varrho_f}{2\Delta t}\|\mathbf{u}^{n+1/2}\|_{L^2(\Omega)}^2, \tag{84}$$

and

$$\frac{\varrho_s h_s}{\Delta t}\int_0^L u_2|_\Gamma^n u_2|_\Gamma^{n+1/2}\, dx_1 \leqslant \frac{\varrho_s h_s}{2\Delta t}\|u_2^n\|_{L^2(\Gamma)}^2 + \frac{\varrho_s h_s}{2\Delta t}\left\|u_2^{n+1/2}\right\|_{L^2(\Gamma)}^2. \tag{85}$$

To estimate the last term in (83), we first use the Young's inequality to obtain

$$\int_0^H \bar{p}(t^{n+1})u_1|_{x_1=0}^{n+1/2}dx_2 \leqslant \frac{H}{2\epsilon}|\bar{p}(t^{n+1})|^2 + \frac{\epsilon}{2}\int_0^H |u_1|_{x_1=0}^{n+1/2}|^2 dx_1, \tag{86}$$

and then we use the trace inequality and the Korn's inequality to get

$$\frac{\epsilon}{2}\int_0^H |u_1|_{x_1=0}^{n+1/2}|^2 dx_1 \leqslant \frac{\epsilon C}{2}\|\mathbf{D}(\mathbf{u}^{n+1/2})\|_{L^2(\Omega)}^2, \tag{87}$$

where ϵ and C are positive constants. Using these estimates, choosing $\epsilon = 2\mu/C$, we obtain from (83) the following inequality:

$$\frac{\varrho_f}{2\Delta t}\|\mathbf{u}^{n+1/2}\|_{L^2(\Omega)}^2 + \left(\frac{\varrho_s h_s}{2\Delta t} + D_0\right)\left\|u_2^{n+1/2}\right\|_{L^2(\Gamma)}^2 + \mu\|\mathbf{D}(\mathbf{u}^{n+1/2})\|_{L^2(\Omega)}^2 + D_1\left\|\frac{\partial u_2^{n+1/2}}{\partial x_1}\right\|_{L^2(\Gamma)}^2$$

$$\leqslant \frac{\varrho_f}{2\Delta t}\|\mathbf{u}^n\|_{L^2(\Omega)}^2 + \frac{\varrho_s h_s}{2\Delta t}\left\|u_2^n\right\|_{L^2(\Gamma)}^2 + \frac{HC}{4\mu}|\bar{p}(t^{n+1})|^2. \tag{88}$$

Eq. (88) can be rewritten as

$$\frac{1}{2}E_I^{n+1/2} + D_I^{n+1/2} \leqslant \frac{1}{2}E_I^n + F_I^{n+1} \tag{89}$$

where

$$E_I^k = \frac{\varrho_f}{\Delta t}\|\mathbf{u}^k\|_{L^2(\Omega)}^2 + \frac{\varrho_s h_s}{\Delta t}\|u_2^k\|_{L^2(\Gamma)}^2, \tag{90}$$

$$D_I^k = \mu\|\mathbf{D}(\mathbf{u}^k)\|_{L^2(\Omega)}^2 + D_0\|u_2^k\|_{L^2(\Gamma)}^2 + D_1\left\|\frac{\partial u_2^k}{\partial x_1}\right\|_{L^2(\Gamma)}^2, \tag{91}$$

$$F_I^k = \frac{HC}{4\mu}|\bar{p}(t^k)|^2, \tag{92}$$

are the discrete versions of energy, dissipation and external action in (80)–(82), respectively.

The above inequality provides a control over the norm of the solution of the problem in Step 1 in terms of the initial and boundary data, as desired. We remark that this is a consequence of the boundary condition (70) which comes from the novel splitting of the structure equation. More precisely, we used the kinematic condition to express the structure velocity in terms of the fluid velocity at the boundary, we retained only the velocity terms of the structure dynamics (those involving the displacement will be treated in the next step), and we kept the action of the fluid stresses at the boundary so that, in the weak form, the boundary condition enters in the energy identity with the right sign, in analogy to the continuous level case. We remark here that even if the dissipative effect of the structure viscoelasticity does not appear to be essential for the stability of the scheme, this term is crucial to guarantee the necessary regularity for the trace of the fluid velocity at the boundary.

As mentioned in Section 4, we solve step 2 as a wave equation for η leading to the following problem

$$\varrho_s h_s \frac{\partial^2 \eta}{\partial t^2} + C_0 \eta - C_1 \frac{\partial^2 \eta}{\partial x_1^2} = 0 \quad \text{on } (0,L) \times (t^n, t^{n+1}). \tag{93}$$

Multiplying (93) by $\partial\eta/\partial t$ and integrating over $(0,L)$ we obtain

$$\frac{d}{dt}\mathcal{E}_{II} = 0 \quad \text{for } t \in (t^n, t^{n+1}), \tag{94}$$

where

$$\mathcal{E}_{II} = \varrho_s h_s \left\|\frac{\partial\eta}{\partial t}\right\|_{L^2(0,L)}^2 + C_0\|\eta\|_{L^2(0,L)}^2 + C_1\left\|\frac{\partial\eta}{\partial x_1}\right\|_{L^2(0,L)}^2. \tag{95}$$

It is clear that this step, at the differential level, is energy preserving. We will now obtain a similar identity for the discretized version of the problem, using a second-order finite difference scheme. Let us take a discretization of the interval $(0,L)$ and let us denote by X^k the vector of the values of η at the nodes of the space-discretization at time t^k. Then, for each k we obtain X^{k+1} from

$$\varrho_s h_s \frac{X^{k+1} - 2X^k + X^{k-1}}{\tau^2} + (C_0 I + C_1 A)\frac{X^{k+1} + 2X^k + X^{k-1}}{4} = 0, \tag{96}$$

where A is the matrix representing the discrete derivatives in space, and $\tau = \Delta t/N$ is the time step used in Step 2 (we use $\tau = \Delta t/5$). Following [27], Section 31.5.4.4, we multiply 96 by the "discrete" velocity $(X^{k+1} - X^{k-1})/2\tau$ and we obtain

$$E_{II}^{k+1/2} = E_{II}^{k-1/2}, \quad \text{for } k = 0, 1, \ldots, N-1, \tag{97}$$

where

$$E_{II}^{k+1/2} = \varrho_s h_s \left|\frac{X^{k+1} - X^k}{\tau}\right|^2 + (C_0 I + C_1 A)\left|\frac{X^{k+1} + X^k}{2}\right|^2 \tag{98}$$

is the discrete analog of $\mathcal{E}_{II}$.

In conclusion, in Step 1 the energy of the solution remains bounded, while in Step 2 the energy remains constant, which infers stability to the overall scheme. This result does not depend on the size of the time step, and therefore the kinematically coupled scheme is *unconditionally stable*. In other words, the size of the time step affects the accuracy but not the stability of the scheme.

7. Conclusions

In this work we presented a novel time-splitting scheme for numerical simulation of fluid–structure interaction between blood flow and vascular tissue. This problem is characterized by stability issues for explicit schemes due to the added mass effect, which is of concern, more generally, in fluid–structure interaction problems whenever the fluid and the structure have comparable mass. The proposed scheme features stability properties of implicit schemes at the computational costs of the explicit ones. The main novelty lies in a "clever" use of the kinematic boundary condition and the Lie's time-splitting scheme that enabled a novel splitting of the structure equation into its elastodynamics part and the fluid load part (with viscoelasticity). The fluid load part (with viscoelasticity) is then used as a boundary condition in the fluid flow problem, while the

elastodynamics part is solved separately, using an energy-preserving scheme. This is in contrast with the classical partitioned schemes that simply split the fluid equations from the structure equations.

Our scheme gets around the difficulties associated with the added mass effect in an elegant and efficient way, and it remains modular since fluid solvers and structure solvers (for elastodynamics) can be employed to solve the corresponding sub-problems. Potential drawbacks include first-order accuracy in time, which can be improved by introducing a symmetrized scheme [27], and the fact that the generalization to thick structures is not straight-forward, although research in this direction is under way.

Overall, for problems in blood flow where approximation of the arterial walls using elastic/viscoelastic membrane or shell models is appropriate, the kinematically coupled time-splitting scheme provides an efficient and simple way for the numerical simulation of the underlying fluid–structure interaction problem.

Future research includes comparison in performance with the already existing schemes [3,45], extension to 3D flows, and a treatment of thick structures.

Acknowledgments

References

[1] F. Baaijens, A fictitious domain/mortar element method for fluid–structure interaction, Int. J. Numer. Meth. Fluids 35 (2001) 743–761.
[2] S. Badia, F. Nobile, C. Vergara, Fluid–structure partitioned procedures based on Robin transmission conditions, J. Comput. Phys. 227 (2008) 7027–7051.
[3] S. Badia, A. Quaini, A. Quarteroni, Splitting methods based on algebraic factorization for fluid–structure interaction, SIAM J. Sci. Comput. 30 (4) (2008) 1778–1805.
[4] Y. Bazilevs, V.M. Calo, T.J.R. Hughes, Y. Zhang, Isogeometric fluid–structure interaction: theory algorithms and computations, Comput. Mech. 43 (2008) 3–37.
[5] Y. Bazilevs, V.M. Calo, Y. Zhang, T.J.R. Hughes, Isogeometric fluid–structure interaction analysis with applications to arterial blood flow, Comput. Mech. 38 (4-5) (2006) 310–322.
[6] M. Bercovier, O. Pironneau, Error estimates for finite element method solution of the Stokes problem in primitive variables, Numer. Math. 33 (1979) 211–224.
[7] V.A. Bokil, Computational methods for wave propagation problems on unbounded domains, Ph.D. Thesis, Department of Mathematics, University of Houston, 2003.
[8] E. Burman, M. Fernández, Stabilization of explicit coupling in fluid–structure interaction involving fluid incompressibility, Comput. Methods Appl. Mech. Eng. (2008), doi: 10.1016/j.cma.2008.10.012.
[9] S. Canic, C. Hartley, D. Rosenstrauch, J. Tambaca, G. Guidoboni, A. Mikelic, Blood flow in compliant arteries: an effective viscoelastic reduced model numerics and experimental validation, Ann. Biomed. Eng. 34 (9) (2006) 575–592.
[10] S. Canic, J. Tambaca, G. Guidoboni, A. Mikelic, C. Hartley, D. Rosenstrauch, Blood flow in compliant arteries: an effective viscoelastic reduced model numerics and experimental validation, SIAM J. Appl. Math. 67 (2006) 164–193.
[11] P. Causin, J. Gerbeau, F. Nobile, Added-mass effect in the design of partitioned algorithms for fluid–structure problems, Comput. Methods Appl. Mech. Eng. 194 (2005) 4506–4527.
[12] N. Cavallini, V. Caleffi, V. Coscia, Finite volume and WENO scheme in one-dimensional vascular system modelling, Comput. Math. Appl. 56 (9) (2008) 2382–2397.
[13] M. Cervera, R. Codina, M. Galindo, On the computational efficiency and implementation of block-iterative algorithms for nonlinear coupled problems, Eng. Comput. 13 (6) (1996) 4–30.
[14] G.-H. Cottet, E. Maitre, T. Milcent, Eulerian formulation and level set models for incompressible fluid–structure interaction, ESAIM – Math. Model. Numer. Anal. 42 (3) (2008) 471–492.
[15] S. Deparis, M. Discacciati, G. Fourestey, A. Quarteroni, Fluid–structure algorithms based on Steklov–Poincaré operators, Comput. Methods Appl. Mech. Eng. 195 (2006) 5797–5812.
[16] S. Deparis, M. Fernandez, L. Formaggia, Acceleration of a fixed point algorithm for a fluid–structure interaction using transpiration condition, Math. Model. Numer. Anal. 37 (4) (2003) 601–616.
[17] J. Donea, Arbitrary Lagrangian–Eulerian finite element methods, in: Computational Methods for Transient Analysis, North-Holland, Amsterdam, 1983, pp. 473–516.
[18] H. Fang, Z. Wang, Z. Lin, M. Liu, Lattice Boltzmann method for simulating the viscous flow in large distensible blood vessels, Phys. Rev. E 65 (2002) 051925.1–051925.11.
[19] L. Fauci, R. Dillon, Biofluidmechanics of reproduction, Ann. Rev. Fluid Mech. 38 (2006) 371–394.
[20] Z.-G. Feng, E. Michaelides, The immersed boundary-Lattice Boltzmann method for solving fluid–particles interaction problem, J. Comput. Phys. 195 (2) (2004) 602–628.
[21] M. Fernández, J.-F. Gerbeau, C. Grandmont, A projection semi-implicit scheme for the coupling of an elastic structure with an incompressible fluid, Int. J. Numer. Methods Eng. 69 (4) (2007) 794–821.
[22] M. Fernández, M. Moubachir, A Newton method using exact Jacobians for solving fluid–structure coupling, Comput. Struct. 83 (2-3) (2005) 127–142.
[23] C. Figueroa, I. Vignon-Clementel, K.E. Jansen, T. Hughes, C. Taylor, A coupled momentum method for modeling blood flow in three-dimensional deformable arteries, Comput. Methods Appl. Mech. Eng. 195 (2006) 5685–5706.
[24] A. Fogelson, R. Guy, Platelet-wall interactions in continuum models of platelet thrombosis: formulation and numerical solution, Math. Med. Biol. 21 (2004) 293–334.
[25] L. Formaggia, J.F. Gerbeau, F. Nobile, A. Quarteroni, On the coupling of 3D and 1D Navier–Stokes equations for flow problems in compliant vessels, Comput. Methods Appl. Mech. Eng. 191 (6-7) (2001) 561–582.

[26] J. Gerbeau, M. Vidrascu, A quasi-Newton algorithm based on a reduced model for fluid–structure interactions problems in blood flows, Math. Model. Numer. Anal. 37 (4) (2003) 631–648.
[27] R. Glowinski, Finite element methods for incompressible viscous flow, in: P.G. Ciarlet, J.-L. Lions (Eds.), Handbook of Numerical Analysis, vol. 6, North-Holland, Amsterdam, 2003, pp. 3–1176.
[28] R. Glowinski, E. Dean, G. Guidoboni, H. Juarez, T.-W. Pan, Applications of Operator-Splitting methods to the direct simulation of particulate and free-surface flows and to the numerical solution of the two-dimensional elliptic Monge–Ampère equation, Jpn. J. Indus. Appl. Math. 25 (2008) 1–63.
[29] R. Glowinski, G. Guidoboni, On the preconditioned conjugate gradient solution of a Stokes problem with Robin-type boundary conditions, C.R. Math., in press, doi:10.1016/j.crma.2009.05.014.
[30] R. Glowinski, G. Guidoboni, Hopf bifurcation in viscous incompressible flow down an inclined plane: a numerical approach, J. Math. Fluid Mech. 10 (2008) 434–454.
[31] R. Glowinski, G. Guidoboni, T.-W. Pan, Wall-driven incompressible viscous flow in a two-dimensional semi-circular cavity, J. Comput. Phys. 216 (1) (2006) 76–91.
[32] G. Guidoboni, R. Glowinski, N. Cavallini, S. Canic, S. Lapin, A kinematically coupled time-splitting scheme for fluid–structure interaction in blood flow, Appl. Math. Lett. 22 (2009) 684–688.
[33] P. Hansbo, Nitsche's method for interface problems in computational mechanics, GAMM-Mitt 28 (2) (2005) 183–206.
[34] M. Heil, An efficient solver for the fully coupled solution of large-displacement fluid–structure interaction problems, Comput. Methods Appl. Mech. Eng. 193 (2004) 1–23.
[35] J. Heywood, R. Rannacher, S. Turek, Artificial boundaries and flux and pressure conditions for the incompressible Navier–Stokes equations, Int. J. Numer. Methods Fluids 22 (1996) 325–352.
[36] T. Hughes, W. Liu, T. Zimmermann, Lagrangian–Eulerian finite element formulation for incompressible viscous flows, Comput. Methods Appl. Mech. Eng. 29 (1981) 329–349.
[37] M. Krafczyk, M. Cerrolaza, M. Schulz, E. Rank, Analysis of 3D transient blood flow passing through an artificial aortic valve by Lattice Boltzmann methods, J. Biomech. 31 (5) (1998) 453–462.
[38] M. Krafczyk, J. Tolke, E. Rank, M. Schulz, Two-dimensional simulation of fluid–structure interaction using Lattice Boltzmann methods, Comput. Struct. 79 (22–25) (2001) 2031–2037.
[39] A. Leuprecht, K. Perktold, M. Prosi, T. Berk, W. Trubel, H. Schima, Numerical study of hemodynamics and wall mechanics in distal end-to-side anastomoses of bypass grafts, J. Biomech. 35 (2) (2002) 225–236.
[40] S. Lim, C. Peskin, Simulations of the whirling instability by the Immersed Boundary Method, SIAM J. Sci. Comput. 25 (2004) 2066–2083.
[41] G. Marchuk, Splitting and alternating direction methods, in: P.G. Ciarlet, J.-L. Lions (Eds.), Handbook of Numerical Analysis, vol. I, North-Holland, Amsterdam, 1990, pp. 197–462 (Chapter 3).
[42] H. Matthies, J. Steindorf, Numerical efficiency of different partitioned methods for fluid–structure interaction, Z. Angew. Math. Mech. 2 (80) (2000) 557–558.
[43] L. Miller, C. Peskin, A computational fluid dynamics study of 'clap and fling' in the smallest insects, J. Exp. Biol. 208 (2) (2005) 195–212.
[44] F. Nobile, Numerical approximation of fluid–structure interaction problems with application to haemodynamics, Ph.D. Thesis, EPFL, Switzerland, 2001.
[45] F. Nobile, C. Vergara, An effective fluid–structure interaction formulation for vascular dynamics by generalized Robin conditions, SIAM J. Sci. Comput. 30 (2) (2008) 731–763.
[46] T.-W. Pan, R. Glowinski, A projection/wave-like equation method for the numerical simulation of incompressible viscous fluid flow modeled by Navier–Stokes equations, Comput. Fluid Mech. J. 9 (2000) 28–42.
[47] C. Peskin, Numerical analysis of blood flow in the heart, J. Comput. Phys. 25 (1977) 220–252.
[48] C. Peskin, D.M. McQueen, A three-dimensional computational method for blood flow in the heart – I immersed elastic fibers in a viscous incompressible fluid, J. Comput. Phys. 81 (2) (1989) 372–405.
[49] A. Quaini, A. Quarteroni, A semi-implicit approach for fluid–structure interaction based on an algebraic fractional step method, Math. Models Methods Appl. Sci. 17 (6) (2007) 957–983.
[50] A. Quarteroni, M. Tuveri, A. Veneziani, Computational vascular fluid dynamics: problems models and methods, Comput. Visual. Sci. 2 (2000) 163–197.
[51] P.L. Tallec, J. Mouro, Fluid–structure interaction with large structural displacements, Comput. Methods Appl. Mech. Eng. 190 (2001) 3039–3067.
[52] R. van Loon, P. Anderson, J. de Hart, F. Baaijens, A combined fictitious domain/adaptive meshing method for fluid–structure interaction in heart valves, Int. J. Numer. Meth. Fluids. 46 (2004) 533–544.
[53] A. Veneziani, Boundary conditions for blood flow problems, Proc. Enumath 97 (1998).
[54] S. Zhao, X. Xu, M. Collins, The numerical analysis of fluid–solid interactions for blood flow in arterial structures Part 2: development of coupled fluid-solid algorithms, Proc. Instn. Mech. Eng. Part H 212 (1998) 241–252.